Explosive felsic eruptions on ocean islands: a case study from Ascension Island (South Atlantic)

Katie Preece[1*], Jenni Barclay[2], Richard J. Brown[3], Katy J. Chamberlain[4], Darren F. Mark[5,6]

1. Department of Geography, Faculty of Science and Engineering, Swansea University, Singleton Park, Swansea, SA2 8PP, UK
2. School of Environmental Sciences, University of East Anglia, Norwich, NR4 7TJ, UK
3. Department of Earth Sciences, Durham University, Science Labs, Durham, DH1 3LE, UK
4. Environmental Sciences Research Centre, University of Derby, Derby, DE22 1GB, UK
5. Scottish Universities Environmental Research Centre, Rankine Avenue, East Kilbride, G75 0QF, UK
6. Department of Earth & Environmental Science, University of St Andrews, St Andrews, KY16 9AJ, UK

* Corresponding Author

Email Address: k.j.preece@swansea.ac.uk

Submitted to Journal of Volcanology and Geothermal Research

Abstract

Ocean island volcanism is generally considered to be dominated by basaltic eruptions, yet felsic products associated with more hazardous explosive eruptive events are also present in the geological record of many of these islands. Ascension Island, recently recognised as an active volcanic system, exhibits explosive felsic eruption deposits but their age, eruptive styles and stratigraphic association with mafic volcanism are thus far unclear. Here we present a felsic pyroclastic stratigraphy for Ascension Island, supplemented by 26 new $^{40}Ar/^{39}Ar$ ages and whole rock geochemical XRF data. More than 80 felsic pyroclastic eruptions have occurred over the last ~ 1 Myr, including subplinian and phreatomagmatic eruptions, which produced pumice fall and pyroclastic density current deposits. Detailed sampling suggests felsic events are unevenly distributed in space and time. Subaerial activity can be divided into four Periods: Period 1 (~1000 – 500 ka) felsic and mafic eruptions, with felsic explosive eruptions, linked to a Central Felsic Complex; Period 2 (~ 500 – 100 ka) mafic period; Period 3 (~ 100 – 50 ka) felsic eruptions associated with the Eastern Felsic Complex; Period 4 (< 50 ka) mafic eruptions. The last explosive eruption occurred at ~ 60 ka. This work highlights the cyclical nature of ocean island volcanism and the timescales over which changes between predominantly mafic and felsic volcanism occur. The prevalence of past felsic explosive eruptions on Ascension highlights the need to consider the possibility of future subplinian or phreatomagmatic events in hazard management plans, with any potential risk compounded by Ascension's small size and remote location.

Keywords: Ascension Island, pyroclastic eruption, volcanic stratigraphy, $^{40}Ar/^{39}Ar$ geochronology, volcanic hazards

1.0 Introduction

Ocean island volcanoes are predominantly associated with basaltic magma compositions, producing lava flows and mildly-explosive scoria cones. However, felsic deposits are also present in ocean island geological records, albeit to varying degrees. For example, even dominantly basaltic volcanic islands such as Hawaii and Iceland have produced evolved rocks, and deposits associated with explosive felsic activity (*e.g*. Cousens et al., 2003; Jónasson, 2007; Shea and Owen, 2016). Peralkaline trachytes and rhyolites constitute ~ 80 % of the surface exposure of Socorro Island (Mexico), including deposits linked to caldera formation (Bohrson and Reid, 1997), and peralkaline phonolites make up ~ 65 % of the surface of Ua Pou Island (Marquesas, French Polynesia) (Legendre et al., 2005). Within the Atlantic, extensive felsic deposits have been described on the Canary Islands, with the greatest abundance of felsic rocks on the islands of Gran Canaria and Tenerife, where felsic pyroclastic density current (PDC) and pumice fall deposits are widespread (*e.g*. van den Bogaard, 1998; Kobberger and Schmincke, 1999; Brown and Branney, 2004). In the Azores, felsic magmas have erupted from central volcanoes mostly via subplinian events, as well as lava domes and coulées, in particular on the islands of São Miguel, Terceira and Faial (*e.g*. Guest et al., 1999; Queiroz et al., 2008; Gertisser et al., 2010; Pimentel et al., 2015). The Cape Verde islands are composed of a range of rock types, but the subaerial geology of Brava Island is dominated by phonolitic pyroclastic products, lava domes and lava flows (*e.g.* Madeira et al., 2010). Felsic magmas can erupt effusively or explosively, generating multiple hazards. Importantly, explosive felsic eruptions may pose elevated risk to volcanic islands, due to their small size, geographic remoteness and lack of systems for early-warning and hazard management (*e.g.* Komorowski et al., 2016; Wilkinson et al., 2016; Selva et al., 2019). Reconstructing volcanic histories, including understanding the character and timing of previous eruptions, is essential for anticipating likely impacts of future eruptions and for generating long-term hazard assessments (*e.g.* Marzocchi and Bebbington, 2012).

Ascension Island (7°56'S, 14°22'W) is a small (98 km^2) ocean island volcano, located ~ 90 km west of the Mid-Atlantic Ridge. The island is a British Overseas Territory, with a population of ~ 800. The active nature of the island has only recently been revealed, with the last eruption occurring at 0.51 ± 0.18 ka, which produced mafic lava flows and scoria (Preece et al., 2018). Felsic pyroclastic deposits have been noted on Ascension (*e.g*. Nielson and Sibbett, 1996; Kar et al., 1998; Hobson, 2001), and it has been estimated that trachytic and rhyolitic products form 14 % of the surface exposure of the island (Nielson and Sibbett, 1996), with pyroclastic material (pumice and scoria) covering 43 % of the island's surface (Harris et al., 1983). However, the felsic pyroclastic deposits have not been described in detail, and little is known about their age.

In considering Ascension's active volcanic status, small size and isolated nature, it is crucial to gain an understanding of the explosive eruptive history of the island, to better inform hazard assessment. Here we present the first detailed stratigraphy and $^{40}Ar/^{39}Ar$ geochronology of the felsic pyroclastic deposits on Ascension Island. Results show that felsic explosive eruptions have been common during the last 1 Myr, and produced a variety of volcanic hazards. These findings contribute an important insight into the nature and periodicity of felsic pyroclastic eruptions in an ocean island setting. Results create a crucial framework for the anticipation of future hazard and understanding the long-term evolution of the magmatic plumbing system.

2. 0 Background

2.1 Geological Setting

Most previous geological work on Ascension has focused on understanding tectonic association, petrogenesis, and magmatic processes, using geophysical, geochemical and petrological techniques (*e.g.* Weaver et al., 1996; Kar et al., 1998; Klingelhöfer et al., 2001; Paulick et al., 2010; Chamberlain et al., 2016, 2019, 2020). Ascension is located on 5 – 7 Ma oceanic crust (Klingelhöfer et al., 2001; Paulick et al., 2010), situated between the Ascension and Bode Verde fracture zones (Fig. 1). Whilst some studies have linked Ascension with a mantle plume source (*e.g.* Brozena, 1986; Montelli et al., 2006), other geophysical work revealed a crustal structure beneath Ascension which is inconsistent with a hotspot, and a lack of magmatic underplating, instead suggesting an on-axis origin (Klingelhöfer et al., 2001; Evangelidis et al., 2004). Isotopic data point to on-axis growth of the submarine volcanic edifice, with subsequent volcanism continuing off-axis with partial melting of an enriched mantle source producing the subaerial portion of the island (Paulick et al., 2010).

Early descriptions of the general geology of Ascension are given in Daly (1925), Atkins et al. (1964) and Nielson and Sibbett (1996). Ascension shows a large diversity of erupted products, in terms of both geochemical composition and eruptive style, including voluminous production of felsic magma which has erupted both effusively and explosively. Ascension volcanic products typically define a transitional to mildly alkaline basalt-hawaiite-mugearite-benmoreite-trachyte-rhyolite series, where (Na_2O – 2) > K_2O (Weaver *et al*., 1996), with the more evolved compositions having a peralkaline character (Jeffery and Gertisser, 2018) (Peralkalinity Index = molar (Na_2O + K_2O)/Al_2O_3 >1). The northern, western and southern portions of the island comprise scoria cones and mafic lava flows (Fig. 1), previously subdivided into three groups on the basis of Zr/Nb (Low, Intermediate and High Zr/Nb) (Weaver et al., 1996). The central and eastern areas of the island are mainly composed of trachyte and rhyolite lava flows, domes and pyroclastic material. The occurrence of felsic rocks on an ocean island volcano received attention from Charles Darwin when he visited Ascension in 1836 as part of the Beagle Voyage (Darwin, 1844). At Ascension, felsic compositions are thought to form via fractional crystallisation from alkali basalt, without magma mixing or crustal assimilation (Weaver et al., 1996; Kar et al., 1998; Jicha et al., 2013; Chamberlain et al., 2016, 2019), and there is evidence that some of these evolved melts were produced and stored within the lower crust (Chamberlain et al., 2020). The felsic products are related to a Central Felsic Complex and an Eastern Felsic Complex (*e.g.* Kar et al., 1998) (Fig. 1).

2.2 Volcanic history and geochronology

$^{40}Ar/^{39}Ar$ geochronology of lavas from a borehole on Ascension, indicates that the shift from submarine to subaerial eruptions occurred at ~ 2.5 Ma (Minshull et al., 2010). However, the oldest dated subaerial deposit exposed at the surface on Ascension is a rhyolite lava flow at Middleton Ridge, which has been dated by the $^{40}Ar/^{39}Ar$ technique at 1094 ± 12 ka (Jicha et al., 2013). A trachyte lava was dated at 1.5 ± 0.2 Ma using the K-Ar technique (Harris et al., 1982), although this age has been questioned by Nielson and Sibbett (1996) who re-dated the lava to 0.6 ± 0.3 Ma, also using the K-Ar technique. The most recent eruptions produced hawaiite and mugearite lava flows and scoria in the north and northwest of the island, dated by the $^{40}Ar/^{39}Ar$ technique at 0.51 ± 0.18 ka, 0.55 ± 0.12 ka and 1.64 ± 0.37 ka (Preece et al., 2018). The subaerial eruptive chronology has previously relied strongly on the $^{40}Ar/^{39}Ar$ dating of lavas and has been divided into five stages: 1) 1094 – 719 ka: comprising Middleton Ridge trachyte and rhyolite lavas; 2) 829 – 652 ka: trachyte situated north and west of Middleton Ridge and mafic lavas; 3) 637 – 602 ka: trachyte domes and flows on the southwest slope of Green Mountain; 4) 589 – 298 ka: mafic volcanism mainly concentrated in the southern half of the island; 5) < 169 ka: Eastern Felsic Complex and Holocene mafic eruptions (Jicha et al., 2013).

Based on field observations and limited dating, Kar et al., (1998) proposed that the Eastern Felsic Complex was probably younger than the Central Felsic Complex. This is in agreement with the stages of Jicha et al., (2013) who dated felsic lava in the Eastern Felsic Complex as young as 52 ± 3 ka. Until now, the pyroclastic products have received little attention. An initial pyroclastic stratigraphy was defined during the course of a palaeomagnetic investigation, which identified five major pyroclastic eruptions (Lower Pumice, Middle Pumice, Upper Pumice 1, 2 and 3) (Hobson, 2001), and only one pumice unit has previously been dated (Kar *et al*., 1998). In order to aid hazard analysis and long-term contingency planning, it is crucial that the full range of eruptive styles on Ascension are understood, and that the timing of explosive eruptions is constrained.

3.0 Methods

3.1 Field data and stratigraphy

During field stratigraphic analysis, lithostratigraphic units were defined based upon observable and distinctive lithological properties (lithofacies) and stratigraphic relations (Murphy and Salvador, 1999; Luchhi et al., 2010; Lucchi, 2013). The lithofacies descriptions and abbreviations are listed in Table 1. Eruption units may be defined as volcanic material emplaced during a single eruptive pulse (activity lasting seconds to minutes), eruptive phase (hours to days) or single eruption that may have lasted days to months and is often composed of multiple eruptive pulses (Fisher and Schmincke, 1984). Single eruption units are key to this study, in order to gain an understanding of the eruptive history in terms of number, style and size of explosive felsic eruptions. On Ascension, many lithostratigraphic units are bounded by unconformities and evidence of hiatuses, in the form of erosion surfaces, angular unconformities, deposition of reworked material, and/or weathering of palaeo-surfaces evidenced by the discoloration of primary clasts. Palaeosols are not common on Ascension. Thus, eruption units have been defined based upon interpretation of observed lithostratigraphic units, coupled with evidence for depositional time gaps. Eruption units found on Ascension include pyroclastic fall units, pyroclastic density current units, and lava flow units, depending upon the interpreted manner of emplacement. Many lithostratigraphic units on Ascension are not traceable or possible to correlate between exposures due to poor preservation, with many units only outcropping in one locality.

3.2 ^{40}Ar/^{39}Ar geochronology

^{40}Ar/^{39}Ar ages were obtained from feldspar phenocrysts. Feldspar phenocrysts in Ascension pumice are mainly oligoclase to anorthoclase ± sanidine. The least evolved sample in this study (Middleton Fall; AI14-459A) contained oligoclase to andesine plagioclase (see Chamberlain et al. (2019) for representative feldspar compositions). Feldspar phenocrysts were separated from fresh juvenile pumice and scoria using the methods of Mark et al. (2017). Briefly, pyroclasts were crushed in a jaw crusher, sieved, washed repeatedly in de-ionized water, before the > 500 – < 710 μm size fractions were magnetically separated to isolate feldspar phenocrysts. The feldspar phenocrysts were leached in an ultrasonic bath in 5% HF for 5 minutes to remove adhering groundmass glass, before being rinsed three times in de-ionized water in an ultrasonic bath. Once dried, the feldspars were passed through a magnetic separator at low speed and low angle of tilt, to remove feldspar phenocrysts with mineral or melt inclusions. Samples were then hand-picked under a binocular microscope to eliminate any remaining crystals containing inclusions and any visibly altered crystals. Pristine crystals were parcelled into Cu packets, or Al discs, stacked in glass vials and sealed in a large glass vial for irradiation. International standard Alder Creek sanidines (ACs; with an age of 1.1891 ± 0.0008 Ma; Niespolo et al., 2017) were used as fluence monitors for J-determination and packaged throughout the stack at known spacing (geometry) in between samples. Samples and standards were irradiated in 3 different batches at the Cd-lined (CLICIT) facility of the Oregon State University (USA) TRIGA reactor, all for 2 hours. J-measurements were obtained using either a MAP 215-50 noble gas mass spectrometer (Mark et al., 2014) or a HELIX-SFT multicollector noble gas mass spectrometer (Pickersgill et al., 2020). Single irradiated crystals (n= 30 per sample) were fused with a CO_2 laser and isotope data were collected using the either a MAP 215-50 noble gas mass spectrometer or a HELIX-SFT multicollector noble gas mass spectrometer that has custom modifications for ^{40}Ar/^{39}Ar geochronology (Mark et al., 2009).

Samples were analyzed in several batches; backgrounds and mass discrimination measurements (via automated analysis of multiple air pipettes) specific to each batch were used to correct the data. Air pipettes were run (on average) after every 4 analyses. Backgrounds subtracted from ion beam measurements were arithmetic averages and standard deviations. Mass discrimination was computed based on a power law relationship (Renne et al., 2009) using the isotopic composition of atmospheric Ar reported (Lee et al., 2006) that has been independently confirmed (Mark et al., 2011). Corrections for radioactive decay of ^{39}Ar and ^{37}Ar were made using the decay constants reported by Stoenner et al. (1965) and Renne and Norman (2001), respectively. Ingrowth of ^{36}Ar from decay of ^{36}Cl was corrected using the ^{36}Cl/^{38}Cl production ratio and methods of Renne et al. (2008) and was determined to be negligible. Argon isotope data corrected for backgrounds, mass discrimination, and radioactive decay and ingrowth are given in Supplementary Material 1. Data plots are shown in Supplementary Material 2.

The samples were analyzed by total fusion and step-heating with a CO_2 laser. The mass spectrometers are both equipped with Nier-type ion sources. The MAP 215-50 data was collected using an analogue electron multiplier detector. The HELIX-SFT utilized a combination of detectors; ^{40}Ar was measured using a Faraday cup equipped with a 10^{12} Ohm amplifier and ^{39}Ar-^{36}Ar was measured using an ion counting electron multiplier. Mass spectrometry in both cases utilized peak-hopping by magnetic field switching for 10 cycles.

Ages were computed from the blank-, discrimination- and decay-corrected Ar isotope data after correction for interfering isotopes based on the following production ratios, determined from fluorite and Fe-doped $KAlSiO_4$ glass: $(^{36}Ar/^{37}Ar)_{Ca} = (2.650 \pm 0.022) \times 10^{-4}$; $(^{38}Ar/^{37}Ar)_{Ca} = (1.96 \pm 0.08) \times 10^{-5}$; $(^{39}Ar/^{37}Ar)_{Ca} = (6.95 \pm 0.09) \times 10^{-4}$; $(^{40}Ar/^{39}Ar)_{K} = (7.3 \pm 0.9) \times 10^{-4}$; $(^{38}Ar/^{39}Ar)_{K} = (1.215 \pm 0.003) \times 10^{-2}$; $(^{37}Ar/^{39}Ar)_{K} = (2.24 \pm 0.16) \times 10^{-4}$, as determined previously for this reactor in the same irradiation conditions (Renne, 2014). Ages and their uncertainties are based on the methods of Renne et al. (2010), the calibration of the decay constant as reported by Renne et al. (2011) and the ACs optimization age (1.1891 ± 0.0009 Ma, 1 sigma) as reported by Niespolo et al. (2017).

Outliers in both single-crystal samples and standards were discriminated using a 3-sigma filter applied iteratively until all samples counted are within 3 standard deviations of the weighted mean ± one standard error. This procedure screened older crystals that are logically interpreted as xenocrysts. No younger outliers were recorded during analysis of all samples. Processing of the data using the *n*MAD approach of Kuiper et al. (2008) has no impact on the probability distribution plots for each sample.

Both the probability spectra and the inverse isochron ages are reported (Table 2), and are indistinguishable from each other. However, for consistency the ages reported in text and figures are probability spectra ages, except in a few samples where the $^{40}Ar/^{36}Ar$ is distinguishable from an atmospheric $^{40}Ar/^{36}Ar$ value of 298.56 ± 0.31 (Lee et al., 2006). In these cases, the inverse isochron age is preferred (Table 2 and Supplementary Materials 1 and 2)

3.3 Whole rock major and trace element XRF

Whole rock pumice compositions were obtained from interior portions of fresh samples, which were washed in Milli-Q water in a sonic bath, dried overnight at > 100°C and powdered in a tungsten carbide mill, before fused glass discs and pressed powder pellets were prepared for major and trace element analysis respectively. X-ray fluorescence (XRF) analysis was carried out using a Bruker AXS S4 Pioneer at the University of East Anglia. Loss on ignition (LOI) was carried out by heating ~ 1 g of sample powder in a furnace at 1050°C for 4 hours.

4.0 Results

Pyroclastic lithologies on Ascension Island are wide-ranging and numerous. Pumice lapilli are abundant, and eruption units may be massive (mpL), stratified (spL) and often containing ashy layers. The pumice is often only moderately sorted and sometimes displays bimodal clasts sizes due to the proximal nature of the units. The thickness of individual eruption units of pumice lapilli range from < 1m, up to tens of metres thick. Pumice lapilli units are interpreted to have formed via pumice fallout during explosive eruptions. Several massive pumice breccia (mpBr) deposits are present, which contain pumice clasts up to > 10 cm in diameter, with unit thicknesses generally ~ 2 – 3 m. These massive pumice breccias are interpreted to be explosion breccias, deposited via pyroclastic fallout proximal to the vent. Multiple massive tuffs (mT), and more commonly, massive lapilli tuffs (mLT) are present, occasionally in association with eutaxitic lapilli tuffs (eLT), ranging in thickness from ~ 10 cm to > 10 m. The mT units are interpreted to represent either ash fall or dilute, ash-rich pyroclastic density current (PDC) deposits. The mLT deposits are interpreted to have formed via PDCs, with lapilli componentry in the mLT units frequently pumice (ignimbrites), or composed of scoria, probably formed from more mafic PDCs. Several massive lithic breccias (mlBr) occur, which are ~ 1 – 5 m thick, interpreted to be explosion breccias, with no evidence of them being linked to ignimbrite or pumice fall deposits. The felsic pyroclastic units are intercalated with lavas and with scoria deposits. For example, scoria lapilli (mscL), scoria breccia (mscBr), and scoria spatter agglomerate (mscAg) are situated in the stratigraphy between felsic pyroclastic lithologies, and represent scoria fall deposits with varying proximity to the vent.

In the central region of the island, an abundance of pyroclastic deposits are exposed in the vicinity of NASA Road, Middleton Ridge, Middleton Valley, within Devil's Riding School, and near the village of Two Boats (Fig. 1). Green Mountain is the highest peak (859 m) on Ascension, located near the centre of island (Fig 1). Green Mountain is densely vegetated, although the cuts on the road to the summit provide access to outcrops. Outcrops along the entire length of the Green Mountain Road have been logged (Fig. 2). Here, multiple normal faults dissect the exposures, sometimes displacing eruptive units to the extent that a continuous stratigraphy is not possible to establish. In the east of the island, abundant felsic pyroclastic units, in addition to felsic lava domes and lava flows are located in the region between Thistle Hill and Upper Valley Crater, Goat Hole Ravine, Echo Canyon, in and around Cricket Valley, near Devil's Cauldron and Spire Beach (Fig. 1).

Based on the stratigraphy and the $^{40}Ar/^{39}Ar$ ages, we firstly sub-divide the observed eruption units into those associated with three distinct time periods (1000 – 500 ka; 500 – 100 ka; < 100 ka) as described below.

4.1 1000 – 500 ka

The deposits produced during this time period are predominantly preserved in the centre of the island. The two oldest dated pyroclastic units in this study (Green Mountain Road 1 and the Middleton Fall) are located within the central region of the island and have ages within uncertainty of each other. The unit Green Mountain Road 1 (‘GMR1’) is located at the base of the Green Mountain Road stratigraphy (Figs. 2 and 3a), dated at 916 ± 20 ka (AI14-551) (Fig. 4a,b), and is a trachytic pumice fall deposit, which is at least 7 m thick, although the base is not exposed. The Middleton Fall (872 ± 81 ka; AI14-459A) is a pumice fall unit located in Middleton Valley (Fig. 1). The Middleton Fall is > 3 m thick, with a mpL base, grading up to become more scoria-rich in the top 1.3 m (Fig. 5 log 17). The benmoreite (Table 3) pumice from the Middleton Fall deposit is notable as it is the least evolved pumice within this study (62.2 wt.% SiO_2 when normalised to 100% on a volatile-free basis; Fig. 6) and it contains phenocrysts of amphibole, the presence of which is rare on Ascension (Chamberlain et al., 2019). Older deposits are present in the stratigraphy, below the Middleton Fall, however they are very weathered and altered, thus were not dated (Fig. 5). Correlation between units in the older portion of the stratigraphic record is not possible, as individual units are often only present in one location and not traceable over wider areas, due to erosion and/or burial by more recent deposits.

The deposit of a pumice-rich PDC (ignimbrite) (‘NASA PDC’) is located on Upper NASA Road and in Middleton Valley, as well as on Green Mountain Road (Figs. 2 and 5). The unit has not been directly dated, but on Upper NASA Road, it is situated stratigraphically beneath a pumice breccia unit dated at 793 ± 8 ka (AI14-498F) (Figs. 4c,d and 5). On Upper NASA Road, the ~ 2 m thick ‘NASA PDC’ unit is characterised by pumice fall (mpL) at the base which grades into PDC deposit (mLT) (Fig. 7a), although only the PDC facies is present in Middleton Valley and on Green Mountain Road. The ignimbrite facies is characterised by its orange and white colour, elongated pumice at the base, and lithic clasts of lava, scoria and plutonic cumulates. On Green Mountain Road, the unit is present in several locations, occurring as an orange- and white-coloured massive lapilli tuff or eutaxitic massive lapilli tuff (mLT/emLT) (Fig. 2). On Green Mountain Road, it ranges in thickness from 11 cm to ~ 2 m. Here, the thickest occurrence is on the Residency Track (Fig. 3b), where the deposit displays an erosive base, and contains pumice fiamme. In other localities on Green Mountain Road, the deposit displays a eutaxitic texture, and a jointed top, representing cooling fractures. Another notable PDC deposit in the Middleton area is variably welded, displaying a eutaxitic texture, and is present only near Middleton Ridge (Fig. 7b). Fiamme of pumice and lithic clasts are prevalent towards the base of the unit, with the degree of welding upwardly decreasing. Towards the top of the unit, clasts of pumice, as well as lithic clasts of lava, oxidised lava and cumulate fragments, are supported in a white ashy matrix, which is overlain by a pumice fall, probably related to the same eruption. This unit is undated, but is older than ~ 600 ka.

Several thick pumice fall deposits are present within the central area of Ascension, many of which are present within the stratigraphy on NASA Road and can be correlated to closely surrounding areas (Fig. 5). Overlying a scoria fall deposit at the base of the Lower NASA Road stratigraphy (Figs. 5 and 7c) is a 4 m thick, stratified pumice fall, containing a 6 cm ashy horizon rich in accretionary lapilli ('NASA Rd A'), and is dated at 667 ± 13 ka (AI14-488B). Whole rock geochemical data suggests that this fall deposit may be zoned, with rhyolitic compositions towards the base and trachytic pumice near the top (Table 3 and Fig. 6). The pumice at the surface of NASA Rd A is yellow-coloured and weathered, suggesting a hiatus before the next eruption. Overlying NASA Rd A, is a 10.4 m thick stratified pumice fall with ashy layers ('NASA Road B') (Fig. 7c), which may correlate to a fall deposit on Upper NASA Road dated at 664 ± 7 ka (AI16-708) (Fig 5).

The Goat Hole Ravine 1 ('GHR1') unit is of a similar age and is the oldest dated deposit found in the east of Ascension. GHR1 is a > 14 m thick, stratified pumice lapilli (spL) situated at the base of the Goat Hole Ravine sequence (605 ± 11 ka; AI15-630) (Figs. 8 and 9a). The white trachyte (Table 3 and Fig. 6) pumice clasts often contain pink interiors, and some display a brecciated texture, where fragmentation and annealing have occurred in the conduit. The deposit contains abundant (up to ~ 40 %) lithic clasts, mainly comprising oxidised red scoria, with lesser amounts of mafic lava and plutonic cumulate clasts. This unit has not been correlated with any others on the island. In Goat Hole Ravine, it is unconformably overlain by a breccia (pscBr) composed of pumice and scoria ('Pumice Scoria Breccia') (Fig. 8). Juvenile clasts of pumice and scoria are generally < 10 cm in diameter, but scoria bombs up to ~ 50 cm occur. Clasts of obsidian and plutonic cumulates also characterise this unit. This distinctive unit correlates with deposits on Green Mountain Road, which have been dated at 634 ± 63 ka (AI14-550). On Green Mountain Road, the 'Pumice Scoria Breccia' unit overlies Green Mountain Road 1 in two locations (Fig. 2). On Green Mountain Road, the Pumice Scoria Breccia is thicker (> 10 m) than in Goat Hole Ravine, and contains spatter-like scoria clasts, indicating the eruption origin is probably more proximal to Green Mountain Road than Goat Hole Ravine (Fig. 3c).

A distinctive unit in the central region is the 'Mingled Fall' deposit, which has been described by Chamberlain et al. (2020), in relation to its geochemistry and melt inclusion volatiles, which suggest rhyolite generation in the lower crust. This unit comprises a cm-thick basal ash layer, overlain by mingled pumice clasts and gradually grades upwards to become more scoria-dominated (Fig. 7d). This eruption unit occurs within the Lower NASA Road sequence, and can be correlated to the hills around Upper NASA Road, Pyroclastic Plain, Middleton Valley, and to the Green Mountain Road sequence (Fig. 5). The Mingled Fall deposit is present in two places on Green Mountain Road, most notably on the Residency Track, where it reaches its maximum thickness of 4 m and overlies the NASA PDC (Figs. 2 and 3b). Although it has not been directly dated, on Lower NASA Road it sits stratigraphically between a pumice breccia dated at 693 ± 47 ka (AI14-491) and the NASA Road E pumice fall (591 ± 17 ka; AI14-493A) (Fig. 7e).

NASA Road E pumice fall is the widest correlated unit in the central area of the island. The thickest occurrence is on Lower NASA Road, where the fall deposit is ~ 35 m thick (Figs. 5 and 7e). It is one of the most prominent units on Green Mountain Road, where it is at least 20 m thick, although the top has been eroded and reworked (Figs. 2 and 3d). Based on field characteristics, stratigraphic position and $^{40}Ar/^{39}Ar$ geochronology, it can also be correlated to pumice lapilli deposits in Middleton Valley, Middleton Ridge, Two Boats, and the base of the sequence inside Devil's Riding School (Fig. 5). The pumice lapilli is stratified (spL) and interbedded with cm-thick, pink and yellow-coloured ashy layers. The whole rock SiO_2 content decreases throughout the unit, with rhyolitic pumice near the base and trachytic pumice towards the top (Table 3). As well as the sample from Lower NASA Road, which has been dated at 591 ± 17 ka (AI14-493A), the corresponding pumice on Green Mountain Road (AI16-714), as well as the pumice fall at the base of the Devil's Riding School sequence (AI16-713) (Fig. 7f) have also been dated, which are the same age within uncertainty as the main Lower NASA Road deposit (Table 2). In comparison, Kar et al. (1998) obtained an age of 610 ± 20 ka for the Devil's Riding School pumice, which is the same age, within uncertainty, as the age from this study.

A noteworthy unit stratigraphically above NASA Road E in Devil's Riding School, is the 'Devil's Eyeballs PDC' (Fig. 5). This unit comprises ~ 60 cm of cream-coloured ash with matrix-supported lenses of pumice lapilli (mLT), overlain by an 80 cm bed of yellow-orange ash and pumice lapilli containing very large (~ 3 cm diameter) concretions, known locally on Ascension as 'devil's eyeballs' (Fig. 7g). The top of the unit is composed of creamy-yellow ash, with lenses of pumice, probably reworked by water. This unit tentatively correlates with a unit comprising several interbedded pumice lapilli and ash-rich lapilli tuff layers, situated on Pyroclastic Plain (Fig. 7h), dated at 550 ± 23 ka (AI16-710) and is one of the youngest felsic pyroclastic deposits in the central stratigraphy. Both occurrences are overlain by a 1 – 2 m massive scoria fall (mscL) unit, of unknown origin.

In the east, there are multiple felsic pyroclastic deposits which erupted ~ 500 kyr ago. This is particularly apparent in the area between Thistle Hill and Upper Valley Crater (Fig. 9b). Here, 14 pumice units occur at the base of the stratigraphy, the majority of which erupted around 500 kyr ago (Fig. 8, log 29). Within this sequence, most of the units are pyroclastic fall units composed of trachytic or rhyolitic pumice lapilli (mpL, spL, dspL, bpL, fpL), with some units containing horizons of tuff (mT, //sT), with evident bomb sag features in the lowermost stratigraphic unit in this area (Fig. 8, log 29). Within the sequence, four units have been dated at 549 ± 6 ka, 538 ± 14 ka, 505 ± 40 ka, 516 ± 12 ka (Fig. 8). In addition, the 'North Green Mountain' pumice is present on the northern side of Green Mountain and in Upper Valley Crater, dated at 530 ± 39 ka (AI14-508) (Fig. 8). This deposit comprises trachytic pumice lapilli fall which is white, pink, or dark grey in colour, and some individual clasts display more highly vesicular pink regions, and less vesicular dark grey portions. Above the pumice lapilli is a horizon of welded and eutaxitic clasts interpreted to be a welded fall deposit (Fig. 9c). In Upper Valley Crater, the pumice lapilli are overlain by an ashy layer rich in accretionary lapilli, which grades up into the welded layer.

4.2 500-100 ka

Notably, there are no dated pyroclastic units between ~ 500 and 100 ka, and few pyroclastic deposits present within the stratigraphy which could have been emplaced during this time period. There are four thin (< 1.3 m) pumice deposits near Thistle Hill which remain undated, but stratigraphically overlie a pumice fall dated at 516 ± 12 ka (AI14-532) (Fig. 8 log 29). Based on the abundant deposits in this region which erupted in close succession (Fig. 8

log 29), it is probable that these deposits were emplaced close to ~ 500 ka. Based on the stratigraphy, two prominent eruptions which did occur between 500 and 100 ka are the Green Mountain Scoria and the Cricket Valley eruption.

The Green Mountain Scoria is present in the area between Thistle Hill and Upper Valley Crater, as well as near the base of Cricket Valley, and near the summit of Green Mountain. The summit of Green Mountain is composed of the eroded remnants of a scoria cone and represents the proximal facies and vent region of the Green Mountain Scoria eruption. In Thistle Hill – Upper Valley Crater and Cricket Valley, the deposit is a > 2 m thick, massive to stratified scoria lapilli (mscL, sscL) fall unit, characterized by plutonic lithic clasts (Fig. 8). Associated with this unit is a debris avalanche deposit, which occurs from the northern side of Green Mountain, with the toe located at the aerial masts near Butt Crater (Figs. 1 and 9b). The debris avalanche is composed of Green Mountain scoria, and directly overlies primary Green Mountain scoria fall (Fig. 9d), so probably occurred close to the time of eruption. The boundary between primary scoria fall and the base of the debris avalanche deposit can be defined by a ~ 3 cm thick layer of finely ground and indurated (but not welded) scoria with slickensides.

Cricket Valley is an elongate crater with pyroclastic deposits around the edge. The Green Mountain Scoria is deposited at the base of the sequence within Cricket Valley, overlain by a ~ 1.5 m thick mafic lava flow, and the ‘Cricket Valley’ pyroclastic deposits (Fig. 8). The ‘Cricket Valley pyroclastics’ have been previously described by Nielson and Sibbett (1996), who recorded a thick sequence, with scoria lapilli at the base, overlain by a lithic explosion breccia and then topped by laminated and cross bedded ash layers. We record a similar sequence, comprising 16.5 m of red-orange coloured massive and stratified scoria lapilli and ash, which is likely reworked towards the top. This is overlain by a 16 cm thick massive pumice lapilli (mpL) fall unit, also recorded by Nielson and Sibbett (1996). Overlying this is a lithic breccia (mlBr), containing blocks of mafic and trachytic lava, pumice, oxidised scoria, and plutonic fragments. Bombs and bomb sag features are prevalent, with bombs up to ~ 1.5 m in diameter (Fig. 9e). The lithic breccia is overlain by parallel- and cross-stratified ash (//sT, xsT) layers, containing pumice lenses, likely deposited by dilute PDCs (surges) (Figs. 8 and 9f). In total, the explosion breccia and surge layers are 25.5 m thick. Although the whole sequence has previously been termed 'Cricket Valley pyroclastics' (Nielson and Sibbett, 1996), it is likely to have formed via multiple eruptions, with the lithic breccia and surge layers potentially associated with an eruption event which formed the current Cricket Valley crater. The pumice fall present between the red-orange scoria and the lithic breccia likely originates from elsewhere on the island, and although remains uncorrelated, it represents a time gap between the emplacement of the scoria lapilli unit and the lithic breccia unit.

4.3 < 100 ka

There are multiple explosive eruptions which occurred ~ 100 ka, predominantly within the eastern region of Ascension. The compositionally 'Zoned Fall' deposit is composed of trachytic pumice lapilli at the base, gradually grading into basaltic trachy-andesite scoria lapilli at the top of the unit (Chamberlain et al., 2016). This distinctive unit (Fig. 9g) is exposed in Upper Valley Crater, the area between Upper Valley Crater and Thistle Hill, and at the NE coast (e.g. Hummock Point, Echo Canyon). This unit is also found in more central localities near Pyroclastic Plain and NASA Road, where it stratigraphically overlies the NASA Road stratigraphy (Fig. 5 log 13). The unit thickens and coarsens towards the vent location, which is a fissure located near the NE coast (Fig. 8 log 27 and Fig. 9h). This unit has been dated at 109 ± 12 ka (AI14-443) and is the only pumice unit as young as ~100 ka to be found in the central region of the island. Another unit of a similar age, is the 'Spire Beach' eruption, dated at 106 ± 8 ka (AI14-434). This is a 28 m thick sequence of pumice lapilli and ash beds, with frequent bomb sag features and lithic-rich (up to ~ 70% lithic clasts) horizons. This unit is not traced to elsewhere on the island and represents the remnants of a tuff cone (Figs. 8 and 9i).

The youngest felsic pyroclastic deposits on Ascension Island occur in the east, with several eruptions dated at ~ 60 ka. The trachytic 'Echo Canyon' eruption (59 ± 4 ka; AI15-602A) (Fig. 4e,f) is often exposed stratigraphically above the Zoned Fall deposit (Fig. 8), and is present along the NE coast (Fig. 9h) and near Spire Beach, with the thickest deposit located within Echo Canyon. Within Echo Canyon, the sequence is ~ 50 m thick and broadly comprises pumice lapilli beds (fall) at the base, overlain by a lapilli tuff with bomb sags, further pumice lapilli, baked pink-orange pumice lapilli, and a layer of welded pumice fall (Fig. 9j). The pumice clasts are variably vesiculated, comprising clasts of grey relatively low-density pumice and green-grey micro-vesicular pumice (Fig. 9k). The pumice is characterised by the presence of distinctive feldspar phenocrysts up to 3 – 4 mm in diameter, larger than in other pumice deposits on Ascension. Along the NE coast, the Echo Canyon eruption is represented by massive lapilli tuffs (ignimbrites), sometimes containing accretionary lapilli and beds of pumice and lithic breccia. Within the 'Fissure Area' (Fig. 8 log. 27 and Fig. 9h), the Echo Canyon pumice deposits appear in association with a lava dome and dome talus, which may represent the later effusive stages of the Echo Canyon eruption.

The Echo Canyon eruption deposit is directly overlain by a thick felsic lava flow, the 'Ariane lava' flow (Fig. 1). Dating of this lava flow has been unsuccessful (29 ± 30 ka; AI14-485), with the presence of excess argon ($^{40}Ar/^{36}Ar = 337$), and previous attempts have not yielded sufficient argon to obtain an age (Nielson and Sibbett, 1996). Jicha et al. (2013) obtained an age of 169 ± 43 ka, which is inconsistent with multiple ages in this study, although the reason is not clear. Directly overlying the Ariane lava is the 'Devil's Cauldron' eruption unit, dated at (64 ± 7 ka; AI14-509), implying close timing of the Echo Canyon, Ariane, and Devil's Cauldron eruptions. The most complete, or key section of the 'Devil's Cauldron' unit is exposed on top of the Ariane lava flow, where the unit is 16 m thick (Figs. 8 and 9l). At the base, the unit is ash-rich and dominantly composed of small (< 5 mm) angular clasts of trachyte lava and abundant accretionary lapilli, with some pumice and clasts of obsidian. Pumice lapilli-dominated beds gradually become prevalent at ~ 5m height from the base, with lithic clast content ranging from ~10 – 30 %, comprising clasts of black and red oxidised mafic lava, and obsidian. Clast-supported pumice lapilli layers are interbedded with ash-rich layers, containing accretionary lapilli, bombs and bomb sag features. Towards the top of the deposit, rhyolitic pumice has varying vesicularity, with both micro-vesicular and vesicular grey pumice clasts present. The lithic clasts near the top of the deposit consist of black and red oxidised mafic lava, trachyte lava, and plutonic fragments. To the west of this key section, the Devil's Cauldron unit is present at the top of the Goat Hole Ravine sequence as interbedded layers of accretionary lapilli and pumice lapilli. Further west, between Upper Valley Crater and Thistle Hill, the corresponding deposits consist of 2 – 3 m of ash and accretionary lapilli. To the southeast of the key section, near the Spire Beach Track (Fig. 8), the same unit contains ash and abundant accretionary lapilli at the base, but is dominantly lithic-rich pumice and micro-vesicular pumice lapilli, similar to the upper portions of the main deposit.

5.0 Discussion

5.1 Felsic pyroclastic stratigraphy and correlations

The preservation of the pyroclastic deposits on Ascension Island is variable. Many of the units, especially older deposits, cannot be traced and often crop out in a single location, uncorrelated to other localities. Even the most extensive units are restricted to small portions of the island, correlated between few localities in close (max. ~ 3 – 4 km) proximity of each other. The climate across Ascension varies, with persistent east-southeast trade winds resulting in heavy precipitation in the southeast, and much drier conditions in the rain shadow of Green Mountain, in the north and northwest of the island (Nielson et al., 1996). Rainfall tends to occur as short periods of heavy precipitation, leading to flash floods and erosion *(e.g.* Rosenbaum, 1992). It is therefore probable that pyroclastic deposits have been subject to high rates of erosion, due to heavy rainfall and flash flooding. The prevailing trade wind direction is evident in the shape of scoria cones and scoria distribution, and it is likely that felsic pyroclastic material would also be predominantly dispersed towards the northwest, with a portion deposited in the ocean. Pyroclastic deposits may have been subsequently buried by lava flows on the north and western flanks of the island, many of which are younger than the felsic pyroclastic material (Jicha et al., 2013; Preece et al., 2018).

There are limited stratigraphic correlations between pyroclastic units deposited in the central and eastern localities, with only the Zoned Fall deposit correlated between the two regions. Pyroclastic units within the sequence on Green Mountain Road (Fig. 2) can be correlated with some central and early eastern units. The 'Mingled Fall, 'NASA PDC' and 'NASA Road E' units can be correlated between the central localities and Green Mountain Road, whereas the 'Pumice Scoria Breccia' crops out in the east and in the Green Mountain Road sequence. In the central region of the island, evidence of vent location is limited, but Devil's Riding School, Green Mountain and Middleton Ridge are all probable vents for central deposits. Within this region, individual pyroclastic eruptions have not been linked to a specific vent location due to limited outcrop locations hindering the production of meaningful isopach or isopleth maps. The vent localities for the older eastern deposits are not known, however they may originate from the central region of the island. For example, units such as the 'Pumice Scoria Breccia' and the 'North Green Mountain' appear to be more proximal closer to Green Mountain. The younger eastern deposits can confidently be linked to eastern vent locations. The 'Zoned Fall' originated from a fissure near the NE Coast (Fig. 9h), the 'Spire Beach' tuff cone remnants are situated close to the vent, the 'Echo Canyon' eruption likely originated from near the site of the Echo Canyon dome near the NE coast (Fig. 9h), and the 'Devil's Cauldron' eruption probably erupted from Devil's Cauldron crater. However, the preservation state, the fact that deposits are proximal with any distal material deposited at sea, and the lack of definite vent locations for the majority of eruptions, prohibits calculation of eruption volumes and magnitudes.

In terms of their whole rock major element geochemistry (Table 3), pumice from this study is mainly classed as trachyte and rhyolite, according to the total alkali-silica diagram (Le Maitre, 1989) (Fig. 6). Generally, pumice > 500 ka has relatively lower alkali contents for a given SiO_2 content compared to products < 100 ka, caused by a difference in Na_2O contents (Fig. 6). However, this difference in alkali content is likely an alteration effect, with more Na_2O loss in older samples compared to younger samples, rather than a change in magma chemistry between eruptive periods. Although all samples were apparently fresh, many of the pumice samples have high loss on ignition (LOI) values. Similar hydration is recorded in Ascension pumice samples by whole rock major element and $\delta^{18}O$ data, and is accompanied by Na_2O loss when compared to lavas with similar SiO_2 contents (Weaver et al., 1996; Kar, 1997; Kar et al., 1998). The majority of pumice samples in this study are apparently not sodic, and have a peralkalinity index < 1, although this is also likely an artefact of Na loss during alteration (Table 3).

5.2 Felsic explosive eruption chronology – timing and frequency

The subaerial felsic pyroclastic record of Ascension Island spans nearly the last 1 Myr. The oldest dated felsic pyroclastic unit is 916 ± 20 ka, found at the base of the Green Mountain Road stratigraphy (GMR1 pumice fall). This is younger than the oldest subaerial felsic lava flow age, previously dated at 1094 ± 12 ka (Jicha et al., 2013), although there could be further pyroclastic units within the central region which are older, but remain undated due to their weathered nature.

Taking into account stratigraphical and geochronological data, frequent explosive felsic eruptions occurred from 916 ± 20 ka to approximately 500 ka. However, between approximately 500 ka and 100 ka, there was an apparent hiatus in felsic pyroclastic activity. There is a dearth of felsic explosive units emplaced during this time, with only the mafic Green Mountain Scoria eruption, the Cricket Valley eruption, and four small, non-dated and non-correlated pumice eruptions possibly occurring during this period (Fig. 8 logs 29 and 30). This hiatus is particularly apparent in the stratigraphy of the region between Thistle Hill and Upper Valley Crater (Fig. 8 logs 23 and 29). This hiatus can either be explained by the subsequent removal of any felsic explosive deposits which may have been produced during this time period, or alternatively, by a lack of felsic explosive eruptions during this time. The removal of explosive products may, for example, be attributed to a large collapse event. However, there are no deposits preserved on the island, or any geomorphological feature, which can be linked to such a collapse. In addition, there is a lack of evolved lavas produced during this time, with a predominance of basalt, hawaiite and mugearite lavas erupted (Jicha et al., 2013). The lack of felsic explosive and effusive products therefore suggests that the period of ~ 500 – 100 ka was a predominantly mafic stage in the eruption history of Ascension. This is in general agreement with the mafic volcanism phase proposed by Jicha et al. (2013) to have occurred between 589 and 298 ka. This felsic hiatus may define the transition from activity of the Central to the Eastern Felsic Complex. Between ~ 100 ka and 60 ka, at least 11 pumice-forming explosive eruptions occurred on the east of the island, 7 of which have been dated. At approximately 60 ka, the most-recent explosive felsic eruptions occurred. The Echo Canyon (59 ± 4 ka) eruption, and the Devil's Cauldron eruption (64 ± 7 ka), separated by the Ariane lava flow, all erupted near the NE coast within a short period of time, as the ages are indistinguishable within the uncertainty of the $^{40}Ar/^{39}Ar$ measurements. Based on the $^{40}Ar/^{39}Ar$ uncertainties, taking into account the minimum age of the stratigraphically younger Devil's Cauldron eruption and the maximum age of the stratigraphically older Echo Canyon eruption, they erupted within a maximum time period of 6,000 years. Previously published felsic lava ages from the east of the island are as young as 52 ± 3 ka (Jicha et al, 2013).

Based on the new data presented in this study, in conjunction with previously published lava data from Jicha et al. (2013), four eruptive Periods are defined for the subaerial evolution of Ascension (Fig. 10). Here, the term 'Period' is used to denote a volcanic activity unit, characterised by products from eruptive centres over tens of thousands to millions of years. Periods themselves may be part of a larger cycle, during which volcanic centres migrate and geochemical differences may occur (Fisher and Schmincke, 1984; Lucchi, 2013). On Ascension, Period 1 is the time period between ~ 1 Ma and 500 ka, defined from the earliest dated exposed volcanic product (rhyolite lava flow dated at 1094 ± 12 ka; Jicha et al., 2013), to the felsic hiatus. Throughout Period 1, felsic explosive and effusive eruptions occurred, with mafic eruptions also evident within the geological record during this time. Activity during this Period originated from the centre of the island, around Green Mountain, Middleton and Devils Riding School, and therefore the felsic pyroclastics and lavas erupted during this Period are associated with the Central Felsic Complex. Period 2 (~ 500 – 100 ka) is characterised by a scarcity of felsic products, and can be considered a mafic phase in the evolution of the island. Period 3 consists of frequent felsic explosive and effusive eruptions which took place between ~ 100 ka and 50 ka, with few mafic eruptions during this time. Field evidence points to vent locations in eastern areas and therefore the felsic products of Period 3 are associated with the Eastern Felsic Complex. During the time from the start of Period 3 until the most recent felsic pyroclastic eruption (between approximately 100 ka and 60 ka), at least 11 explosive pumice-forming eruptions occurred, with a mean reoccurrence interval of ~ 3.6 kyr. There is no record of a felsic explosive eruption since ~ 60 ka, or a felsic lava flow younger than ~ 50 ka (Jicha et al., 2013), with only mafic eruptions occurring since 50 ka. Given the felsic explosive reoccurrence internal of ~ 3.6 kyr during Period 3, but a lack of any felsic eruption for the last 50 kyr (Fig. 10), the time since 50 ka may be denoted as a new Period (Period 4), dominated by mafic eruptions, as young as 0.51 ± 0.18 ka (Preece et al., 2018).

Cyclic mafic and felsic periods are common features of ocean island volcanism. In ocean islands settings, felsic melt generation is thought to be related to open-system fractional crystallisation processes in the upper crust (< 5 km), with variable contribution from mafic mixing and crustal assimilation (*e.g*. Jeffery and Gertisser, 2018 and references therein). At other Atlantic islands, transitions between mafic and felsic periods can often be linked to caldera formation. For example, Sete Cidades volcano, on São Miguel, Azores, has produced several compositional cycles (Moore, 1991) linked to caldera formation, with post-caldera activity associated with larger proportions of evolved material (*e.g*. Beier et al., 2006). On Gough Island, basaltic volcanism ended with caldera formation, followed by volcanic quiescence during which time fractional crystallisation processes produced subsequently erupted trachytes (Le Maitre, 1960; Chevallier, 1987). On Tenerife, mafic injection into shallow phonolitic reservoirs previously triggered caldera-formation, resulting in the destruction of the shallow reservoir system (*e.g* Triebold et al., 2006). After caldera collapse, a 200 kyr mafic period ensued before phonolitic volcanism recommenced, which is thought to be the time required to form new shallow evolved reservoirs capable of producing repeated phonolitic eruptions (Marti and Gudmundsson, 2000). However, it is difficult to reconcile processes responsible for mafic and felsic periods on other Atlantic islands with processes on Ascension. On Ascension, there is no field evidence of a caldera, and there is evidence that at least some felsic melts evolve via closed-system fractionation within the lower crust, at depths of up to 11 km (Chamberlain et al., 2019; 2020). Potentially the magma reservoir(s) responsible for formation of the Central Felsic Complex ceased being eruptible at ~ 500 ka. Mafic magmatism continued for ~ 400 kyr, whilst new a felsic reservoir(s) assembled beneath the east of the island, with the change in location perhaps induced by changes in the local stress field (*e.g.* Marti and Gudmundsson, 2000). However, the reasons for this remain unclear and warrant further petrological and geophysical investigation.

5.3 Felsic explosive eruption styles and hazards

The felsic pyroclastic deposits demonstrate that various eruptive styles have occurred throughout the last 1 Myr of subaerial activity on Ascension, with evidence of both magmatic and phreatomagmatic activity. The most common type of deposit associated with explosive felsic eruptions on Ascension is pumice fall, as there are at least 73 pumice-bearing fall deposits preserved on Ascension. Many of the pumice fall deposits are indicative of sustained eruption columns, probably of subplinian scale. There are no prominent signs of caldera collapse on Ascension which may be linked to a larger-scale eruption, although there are several lithic breccia units, situated on Green Mountain Road and within the eastern areas. However, the breccia units are localised, with no evidence of being linked to PDC deposits or caldera collapse (e.g. lithic lag breccias), and are therefore more likely to be proximal explosion breccias.

Pyroclastic density current deposits on Ascension include pumice-rich ignimbrites, welded eutaxitic PDC deposits, a dilute surge deposit, as well as scoria-bearing mafic PDC deposits. In total, there is evidence in the stratigraphy for 16 PDC-forming eruptions, with some PDC deposits associated with fall facies. For example, ignimbrites linked to the Echo Canyon eruption, Devil's Eyeball's eruption, NASA PDC eruption, as well as the eutaxtic PDC deposits found at Middleton, are all associated with fall facies produced during these eruptions. Other

PDC deposits are often discrete, weathered, matrix-supported and ash-rich units, not correlated with any other unit. The PDCs formed during the Cricket Valley eruption are the only dilute surge-type deposits on the island. Despite several lava domes situated in the east of Ascension, there are no obvious block-and-ash flow deposits.

Phreatomagmatic deposits are found in the east of the island, including those of the Spire Beach, Cricket Valley and Devils Cauldron eruptions. These deposits contain characteristic phreatomagmatic features such as stratification of ash-rich and clast-rich layers, accretionary lapilli, lithic clast-rich layers, cross-stratification and bomb sag features. In addition, based on field characteristics, two other units near the base of the stratigraphy in the Thistle Hill and Upper Valley Crater regions were likely formed via phreatomagmatic activity, although have not been correlated elsewhere. These eruptions were subaerial, rather than submarine phreatomagmatic eruptions, and therefore the water likely came into contact with the magma via fractures and pores in the wall rock.

In summary, there are > 80 felsic explosive eruptions which erupted over the last 1 Myr, evidenced within the subaerial stratigraphy. This should be regarded as a minimum estimate due to erosion or burial of deposits, and the likelihood that much explosive material is deposited at sea rather than on land.

The lack of felsic eruptions and predominance of mafic eruptions for the last 50 kyr, raises questions about how any possible future eruption may proceed. The most recent eruptions consisted of effusive and mild explosive activity, producing mafic lavas and scoria in the NW of the island (Preece et al., 2018). Based on the most recent activity, it is likely that future volcanic hazards may include lava flows, ballistics, tephra fallout and gas emissions (Preece et al., 2018). However, given the abundance of felsic explosive deposits on the island and previous cyclic activity, the possibility of another similar explosive eruption in the future should not be ruled out. Recent textural observations from the Mingled Fall deposit, suggest that magma can ascend rapidly, in timescales on the order of ~ 24 hours, emphasising the importance of anticipating future activity on Ascension (Chamberlain et al., 2020). If a future subplinian or phreatomagmatic eruption were to occur on Ascension, the entire island would likely be affected by tephra fallout, topographically lower areas may be affected by PDCs, and air travel could be disrupted, with the risk further compounded by Ascension's small size and remote location.

6.0 Conclusions

Throughout the last 1 Myr, felsic eruptions have been commonplace on Ascension Island, linked to a Central Felsic Complex and an Eastern Felsic Complex. Stratigraphic analysis, $^{40}Ar/^{39}Ar$ geochronology and whole rock geochemical data reveal that between ~ 900 and 60 ka, more than 80 explosive felsic eruptions have occurred. Subplinian eruptions generated pumice fall deposits up to ~ 40 m thick, welded fall deposits, ignimbrites and eutaxitic-textured welded PDC deposits. In addition, phreatomagmatic eruptions can be associated with pumice fall, massive lithic breccias, and dilute PDC (surge) deposits. Subaerial activity can be divided into four eruption periods: Period 1 – felsic and mafic eruptions, with felsic explosive eruptions, linked to the Central Felsic Complex (~ 1000 – 500 ka); Period 2 – mafic period with dearth of felsic eruptions (~500 – 100 ka); Period 3 – felsic eruptions associated with the Eastern Felsic Complex (100 – 50 ka); Period 4 – mafic eruptions. Although a felsic explosive eruption hasn't occurred on Ascension for ~ 60 ka, and the most recent eruptions have consisted of basaltic activity, a future explosive felsic eruption cannot be ruled out. These results reveal the cyclical nature of Ascension Island volcanism and the timescales over which changes between predominantly mafic and felsic volcanism occur, pertinent to better understanding ocean island volcanism in general. This study highlights that frequent felsic explosive eruptions, with wide-ranging styles, have taken place on Ascension Island throughout its subaerial history, and therefore the possibility of a similar eruption occurring on Ascension in the future remains possible.

Acknowledgements

We extend special thanks to the late Jon Davidson for dedication to the development and progression of this project, and for stimulating and inspiring discussion. We thank the Ascension Island Government and Conservation Department for permission to carry out the work. Ascension Island Conservation Department, Ascension Island Heritage Society and Drew Avery are thanked for logistical support during fieldwork. Thanks go to Ben Cohen, Anna Hicks, Fin Stuart, Charlotte Vye-Brown and Barry Weaver for valuable discussions and field assistance. We are grateful to Ross Dymock and Jim Imlach for assistance with $^{40}Ar/^{39}Ar$ sample preparation and technical support. Bertrand Lézé is acknowledged for technical assistance with XRF analysis. This work was funded by a Leverhulme Trust Research Project Grant (RPG-2013-042), with support from a Gloyne Outdoor Geological Research award from the Geological Society of London. We thank reviewers Adriano Pimentel and Brian Jicha, for their prompt reviews and constructive comments which helped to improve this manuscript, and we thank Jose Luis Macias for Editorial handling.

References

Ammon, K., Dunai, T.J., Stuart, F.M., Meriaux, A.-S., Gayer, E. (2009) Cosmogenic ^3He exposure ages and geochemistry of basalts from Ascension Island, Atlantic Ocean. Quaternary Geochronology, 4, 525-532.

Atkins, F.B., Baker, P.E., Bell, J.D., Smith, D.G.W. (1964) Oxford expedition to Ascension Island, 1964. Nature, 204, 722-724.

Beier, C., Haase, K.M., Hansteen, T.H. (2006) Magma evolution on Sete Cidades Volcano, São Miguel, Azores. Journal of Petrology, 47, 1375-1411.

Bohrson, W.A., Reid, M.R. (1997) Genesis of silicic peralkaline volcanic rocks in an ocean island setting by crustal melting and open-system processes: Socorro Island, Mexico. Journal of Petrology, 38, 1137-1166.

Branney, M.J., Kokelaar, P. (2002) Pyroclastic density currents and the sedimentation of ignimbrites. Geological Society of London, Memoir 27, 152pp.

Brown, R.J., Branney, M.J. (2004) Event-stratigraphy of a caldera-forming ignimbrite eruption on Tenerife: the 273 ka Poris Formation. Bulletin of Volcanology, 66, 392-416.

Brozena, J.M. (1986) Temporal and spatial variability of seafloor spreading processes in the Northern South Atlantic. Journal of Geophysical Research, 91, 497-510.

Chamberlain, K.J., Barclay, J., Preece, K., Brown, R.J., Davidson, J.D., Edinburgh Ion Microprobe Facility. (2016) Origin and evolution of silicic magmas at ocean islands: perspectives from a zoned fall deposit on Ascension Island, South Atlantic. Journal of Volcanology and Geothermal Research, 327, 349-360.

Chamberlain, K.J., Barclay, J., Preece, K., Brown, R.J., Davidson, J.D. (2019) Lower crustal heterogeneity and fractional crystallisation control evolution of small-volume magma batches at ocean island volcanoes (Ascension Island, South Atlantic). Journal of Petrology, 60, 1489-1522.

Chamberlain, K.J., Barclay, J., Preece, K., Brown, R.J., McIntosh, I., Edinburgh Ion Microprobe Facility. (2020) Deep and disturbed: conditions for formation and eruption of a mingled rhyolite at Ascension Island, south Atlantic. Volcanica, 3, 139-153.

Chevellier, L. (1987) Tectonic and structural evolution of Gough Volcano: a volcanological model. Journal of Volcanology and Geothermal Research, 33, 325-336.

Cousens, B.L., Clague, D.A., Sharp, W.D. (2003) Chronology, chemistry, and origin of trachytes from Hualalai Volcano, Hawaii. Geochemistry Geophysics Geosystems, 4, 1078.

Daly, R.A. (1925) The geology of Ascension Island. Proceedings of the American Academy of Arts and Sciences. 60, 1-80.

Darwin, C.R. (1844) Geological observations on the volcanic islands visited during the voyage of H.M.S. Beagle, together with some brief notices of the geology of Australia and the Cape of Good Hope. Being the second part of the geology of the voyage of the Beagle, under the command of Capt. Fitzroy, R.N. during the years 1832 to 1836. London: Smith Elder and Co.

Evangelidis, C.P., Minshull, T.A., Henstock, T.J. (2004) Three-dimensional crustal structure of Ascension Island from active source tomography. Geophysical Journal International, 159, 311-325.

Fisher, R.V., Schmincke, H.-U. (1984) Pyroclastic Rocks. Springer-Verlag, Berlin, Heidelberg, pp. 472.

Gertisser, R., Self, S., Gaspar, J.L., Kelley, S.P., Pimentel, A., Eikenberg, J., Barry, T.L., Pacheco, J.M., Queiroz, G., Vespa, M. (2010) Ignimbrite stratigraphy and chronology on Terceira Island, Azores. In: Groppelli, G., Viereck-Goette, L. (Eds.) Stratigraphy and Geology of Volcanic Areas: Geological Society of America Special Paper 464, p. 133–154

Guest, J.E., Gaspar, J.L., Cole, P.D., Queiroz, G., Duncan, A.M., Wallenstein, N., Ferreira, T., Pacheco, J.-M. (1999) Volcanic geology of Furnas Volcano, São Miguel, Azores. Journal of Volcanology and Geothermal Research, 92, 1-29.

Harris, C., Bell, J.D., Atkins, F.B. (1982) Isotopic composition of lead and strontium in lava in course-grained blocks from Ascension Island, South Atlantic. Earth and Planetary Science Letters, 60, 79-85.

Harris, C. (1983) The petrology of lavas and associated plutonic inclusions of Ascension Island. Journal of Petrology, 24, 424-470

Hobson, K. (2001) The pyroclastic deposits and eruption history of Ascension Island: a palaeomagnetic and volcanological study. PhD Thesis, University of Oxford.

Jeffery, A.J., Gertisser, R. (2018) Peralkaline felsic magmatism of the Atlantic Islands. Frontiers in Earth Science, 6:145.

Jicha, B.R., Singer, B.S. Valentine, M.J. (2013) $^{40}Ar/^{39}Ar$ geochronology of subaerial Ascension Island and a re-evaluation of the temporal progression of basaltic to rhyolitic volcanism. Journal of Petrology, 54, 2581-2596.

Jónasson, K. (2007) Silicic volcanism in Iceland: Composition and distribution within the active volcanic zones. Journal of Geodynamics, 43, 101-117.

Kar, A. (1997) A comprehensive geological, geochemical, and petrogenetic study of hotspot-related oceanic basaltic-rhyolite series rocks from Ascension Island, South Atlantic Ocean. Unpublished PhD Thesis. University of Oklahoma, USA, 260pp.

Kar, A., Weaver, B., Davidson, J., Colucci, M. (1998) Origin of differentiated volcanic and plutonic rocks from Ascension Island, South Atlantic Ocean. Journal of Petrology, 39, 1009-1024.

Klingelhöfer, F., Minshull, T.A., Blackman, D.K., Harben, P., Chilgers, V. (2001) Crustal structure of Ascension Island from wide-angle seismic data: implications for the formation of near-ridge volcanic islands. Earth and Planetary Science Letters, 190, 41-56.

Kobberger, G., Schmincke, H.-U. (1999) Deposition of rheomorphic ignimbrite D (Mogán Formation), Gran Canaria, Canary Islands, Spain. Bulletin of Volcanology, 60, 465-485.

Komorowski, J.-C., Morin, J., Jenkins, S., Kelman, I. (2016) Challenges of volcanic crises on Small Island States. In: Fearnley, C.J., Bird, D.K., Haynes, K., McGuire, W.J., Jolly, G. (Eds.) Observing the volcano world. Advances in Volcanology (An Official Book Series of the International Association of Volcanology and Chemistry of the Earth's Interior – IAVCEI, Barcelona, Spain). Springer, Cham.

Kuiper, K.F., Deino, A., Hilgen, F.J., Krijgsman, W., Renne, P.R., Wijbrans, J.R. (2008) Synchronizing rock clocks of Earth history. Science, 320, 500-504.

Lee, J.Y., Marti, K., Severinghaus, J.P., Kawamura, K., Yoo, H.S., Lee, J.B., Kim, J.S. (2006) A redetermination of the isotopic abundances of atmospheric argon. Geochimica Cosmochimica Acta, 70, 4507-4512.

Legendre, C., Maury, R.C., Caroff, M., Guillou, H., Cotten, J., Chauvel, C., Bollinger, C., Hémond, C., Guille, G., Blais, S., Rossi, P., Savanier, D. (2005) Origin of exceptionally abundant phonolites on Ua Pou Island (Marquesas, French Polynesia): partial melting of basanites followed by crustal contamination. Journal of Petrology, 46, 1925-1962.

Le Maitre, R.W. (1960) The geology of Gough Island, South Atlantic. Overseas Geology and Mineral Resources, 7, 1309-1340.

Le Maitre, R.W., Bateman, P., Dudek, A., Keller, J., Lameyre, J., Le Bas, M.J., Sabine, P.A., Schmid, R., Sorensen, H., Streckeisen, A., Woolley, A.R., Zanettin, B. (1989) A Classification of Igneous Rocks and Glossary of Terms: Recommendations of the International Union of Geological Sciences Subcommission on the Systematics of Igneous Rocks. Oxford: Blackwell Scientific.

Lucchi, F., Tranne, C.A., Rossi, P.L. (2010) Stratigraphic approach to mapping of the late Quaternary volcanic island of Lipari (Aeolian archipelago, southern Italy). In: Gropelli, G., Viereck-Goette, L. (Eds.) Stratigraphy and geology of volcanic areas: Geological Society of America, Special Paper 464, 1-32.

Lucchi, F. (2013) Stratigraphic methodology for the geological mapping of volcanic areas: insights from the Aeolian archipelago (southern Italy). In: Lucchi, F., Peccerillo, A., Keller, J., Tranne, C.A., Rossi, P.L, (Eds.) The Aeolian Islands Volcanoes. Geological Society, London, Memoirs, 37, 37-53.

Madeira, J., Mata, J., Mourão, C., Brum da Silveira, A., Martins, S., Ramalho, R., Hoffmann, D.L. (2010) Volcano-stratigraphic and structural evolution of Brava Island (Cape Verde) based on $^{40}Ar/^{39}Ar$, U-Th and field constraint. Journal of Volcanology and Geothermal Research, 196, 219-235.

Mark, D.F., Barford, D., Stuart, F.M., Imlach, J. (2009) The ARGUS multicollector noble gas mass spectrometer: Performance for $^{40}Ar/^{39}Ar$ geochronology: Geochemistry Geophysics Geosystems, 10, Q0AA02.

Mark, D.F., Stuart, F.M., de Podesta, M. (2011) New high-precision measurements of the isotopic composition of atmospheric argon. Geochimica Cosmochimica Acta, 75, 7494-7501.

Mark, D.F., Petraglia, M., Smith, V.C., Morgan, L.E., Barford, D.N., Ellis, B.S., Pearce, N.J., Pal, J.N., Korisettar, R. (2014) A high-precision $^{40}Ar/^{39}Ar$ age for the Young Toba Tuff and dating of ultra-distal tephra: forcing of Quaternary climate and implications for hominin occupation of India. Quaternary Geochronology, 21, 90-103.

Mark, D.F., Renne, P.R., Dymock, R.C., Smith, V.C., Simon, J.I., Morgan, L.E., Staff, R.A., Ellis, B.S., Pearce, N.J.G. (2017) High-precision $^{40}Ar/^{39}Ar$ dating of Pleistocene tuffs and temporal anchoring of the Matuyama-Bruhnes boundary. Quaternary Geochronology, 39, 1-23.

Marti, J., Gudmundsson, A. (2000) Las Cañadas caldera (Tenrife, Canary Islands): an overlapping collapse caldera generated by magma-chamber migration. Journal of Volcanology and Geothermal Research, 103, 161-173.

Marzocchi, W., Bebbington, M.S. (2012) Probabilistic eruption forecasting at short and long time scales. Bulletin of Volcanology, 74, 1777-1805.

Minshull, T.A., Ishizuka, O., Garcia-Castellanos, D. (2010) Long-term growth and subsidence of Ascension Island: constraints on the rheology of young oceanic lithosphere. Geophysical Research Letters, 37, L23306.

Montelli, R., Nolet, G., Dahlen, F.A., Masters, G. (2006) A catalogue of deep mantle plumes: New results from finite-frequency tomography. Geochemistry, Geophysics, Geosystems, 7, Q11007.

Moore, R.B. (1991) Geology of three late Quaternary stratovolcanoes on São Miguel, Azores. US Geological Survey Bulletin 1900, US Geological Service.

Murphy, M.A., Salvador, A. (1999) International Stratigraphic Guide – an abridged version. International Subcommission on Stratigraphic Classification of IUGS International Commission on Stratigraphy. Episodes, 22, 255-271.

Nielson, D. L., Sibbett, B.S. (1996) Geology of Ascension Island, South Atlantic Ocean. Geothermics, 25, 427-448.

Nielson, D.L., Adams, M.C., Sibbett, B.S., Wright, P.M. (1996) Shallow thermal structure and hydrology of Ascension Island, South Atlantic Ocean. Geothermics, 25, 521-541.

Niespolo, E., Rutte, D., Deino, A.L., Renne, P.R. (2017) Intercalibration and age of the Alder Creek sanidine $^{40}Ar/^{39}Ar$ standard: Quaternary Geochronology, 39, 205-213.

Paulick, H., Münker, C., Schuth, S. (2010) The influence of small-scale mantle heterogeneities on Mid-Ocean Ridge volcanism: Evidence from the southern Mid-Atlantic Ridge (7°30'S to 11°30'S) and Ascension Island. Earth and Planetary Science Letters, 296, 299-310.

Pickersgill, A.E, Mark, D.F, Lee, M.R., Osinski, G.R. (2020) $^{40}Ar/^{39}Ar$ systematics of melt lithologies and target rocks from the Gow Lake impact structure, Canada. Geochimica et Cosmochimica Acta, 274, 317-332.

Pimentel, A., Pacheco, J., Self, S. (2015) The ~1000 years BP explosive eruption of Caldeira Volcano (Faial, Azores): the first stage of incremental caldera formation. Bulletin of Volcanology, 77, 42.

Preece, K., Mark, D.F., Barclay, J., Cohen, B.E., Chamberlain, K.J., Jowitt, C., Vye-Brown, C., Brown, R.J., Hamilton, S. (2018) Bridging the gap: $^{40}Ar/^{39}Ar$ dating of volcanic eruptions from the 'Age of Discovery', Geology, 46, 1035-1038.

Queiroz, G., Pacheco, J.M., Gaspar, J.L., Aspinall, W.P., Guest, J.E., Ferreira, T. (2008) The last 5000 years of activity at Sete Cidades volcano (São Miguel Island, Azores): implications for hazard assessment. Journal of Volcanology and Geothermal Research, 178, 562-573.

Renne, P.R. (2014) Some footnotes to the optimization-based calibration of the $^{40}Ar/^{39}Ar$ system. Geological Society of London Special Publication, 378, 21-31.

Renne, P.R., Norman, E.B. (2001) Determination of the half-life of ^{37}Ar by mass spectrometry. Physical Review C, 63, 047302.

Renne, P.R., Sharp, Z.D., Heizler, M.T. (2008) Cl-derived argon isotope production in the CLICIT facility of OSTR reactor and effects of the Cl-correction in $^{40}Ar/^{39}Ar$ geochronology. Chemical Geology, 255, 463-466.

Renne, P.R., Cassata, W.S., Morgan, L.E. (2009) The isotopic composition of atmospheric argon and $^{40}Ar/^{39}Ar$ geochronology: time for a change? Quaternary Geochronology, 4, 288-298.

Renne, P.R., Mundil, R., Balco, G., Min, K., Ludwig, K.R. (2010) Joint determination of ^{40}K decay constants and $^{40}Ar^*/^{40}K$ for the Fish Canyon sanidine standard, and improved accuracy for $^{40}Ar/^{39}Ar$ geochronology. Geochimica Cosmochimica Acta, 74, 5349-5367.

Renne, P.R., Mundil, R., Balco, G., Min, K., Ludwig, K.R. (2011) Response to comment by W. H. Schwarz et al. on "Joint determination of ^{40}K decay constants and $^{40}Ar^*/^{40}K$ for the Fish Canyon sanidine standard, and improved accuracy for $^{40}Ar/^{39}Ar$ geochronology". Geochimica Cosmochimica Acta, 75, 5097-5100.

Rosenbaum, M.S. (1992) The geology of Ascension Island. Geology Today, 8, 180-184.

Selva, J., Acocella, V., Bisson, M., Caliro, S., Costa, A., Della Seta, M., De Martino, P., de Vita, S., Frederico, C., Giordano, G., Martino, S., Cardaci, C. (2019) Multiple natural hazards at volcanic islands: a review for the Ischia volcano, Italy. Journal of Applied Volcanology 8:5.

Shea, T., Owen, J. (2016) Discovery of a trachyte ignimbrite sequence at Hualālai, Hawaii. Bulletin of Volcanology, 78, 34.

Stoenner, R.W., Oa, S., Katcoff, S. (1965) Half-lives of Argon-37, Argon-39 and Argon-42. Science, 148, 1325.

Triebold, S., Kronz, A., Wörner, G. (2006) Anorthite-calibrated backscattered electron profiles, trace elements, and growth textures in feldspars from the Teide-Pico Viejo volcanic complex. Journal of Volcanology and Geothermal Research, 154, 117-130.

van den Bogaard, P. (1998) $^{40}Ar/^{39}Ar$ ages of Pliocene-Pleistocene fallout tephra layers and volcaniclastic deposits in the sedimentary aprons of Gran Canaria and Tenerife (Sites 953, 954 and 956). Proceedings of the Ocean Drilling Program, Scientific Results, 157, 329-341.

Weaver, B., Kar, A., Davidson, J., Colucci, M. (1996) Geochemical characteristics of volcanic rocks from Ascension Island, South Atlantic Ocean. Geothermics, 25, 449-470.

Wilkinson, E., Lovell, E., Carby, B., Barclay, J., Robertson, R.E.A. (2016) The dilemmas of risk-sensitive development on a small volcanic island. Resources, 5, 21.

Figures and captions

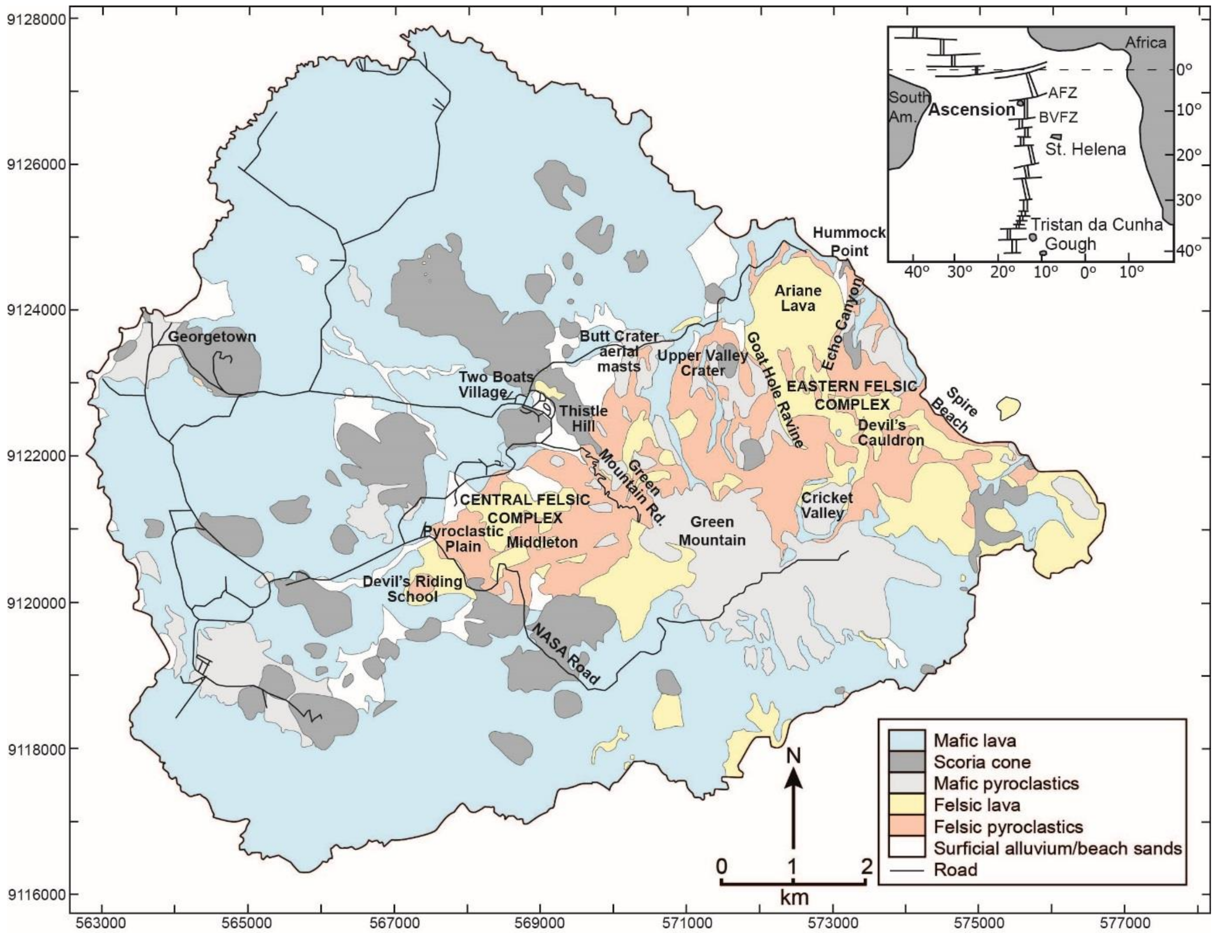

Fig 1: Geological map of Ascension Island (modified after Nielson and Sibbett, 1996), showing roads, settlements and localities referred to in this work. Inset: location map of Ascension at the southern Mid-Atlantic Ridge, between the Ascension Fracture Zone (AFZ) and the Bode Verde Fracture Zone (BVFZ) (modified after Paulick et al., 2010).

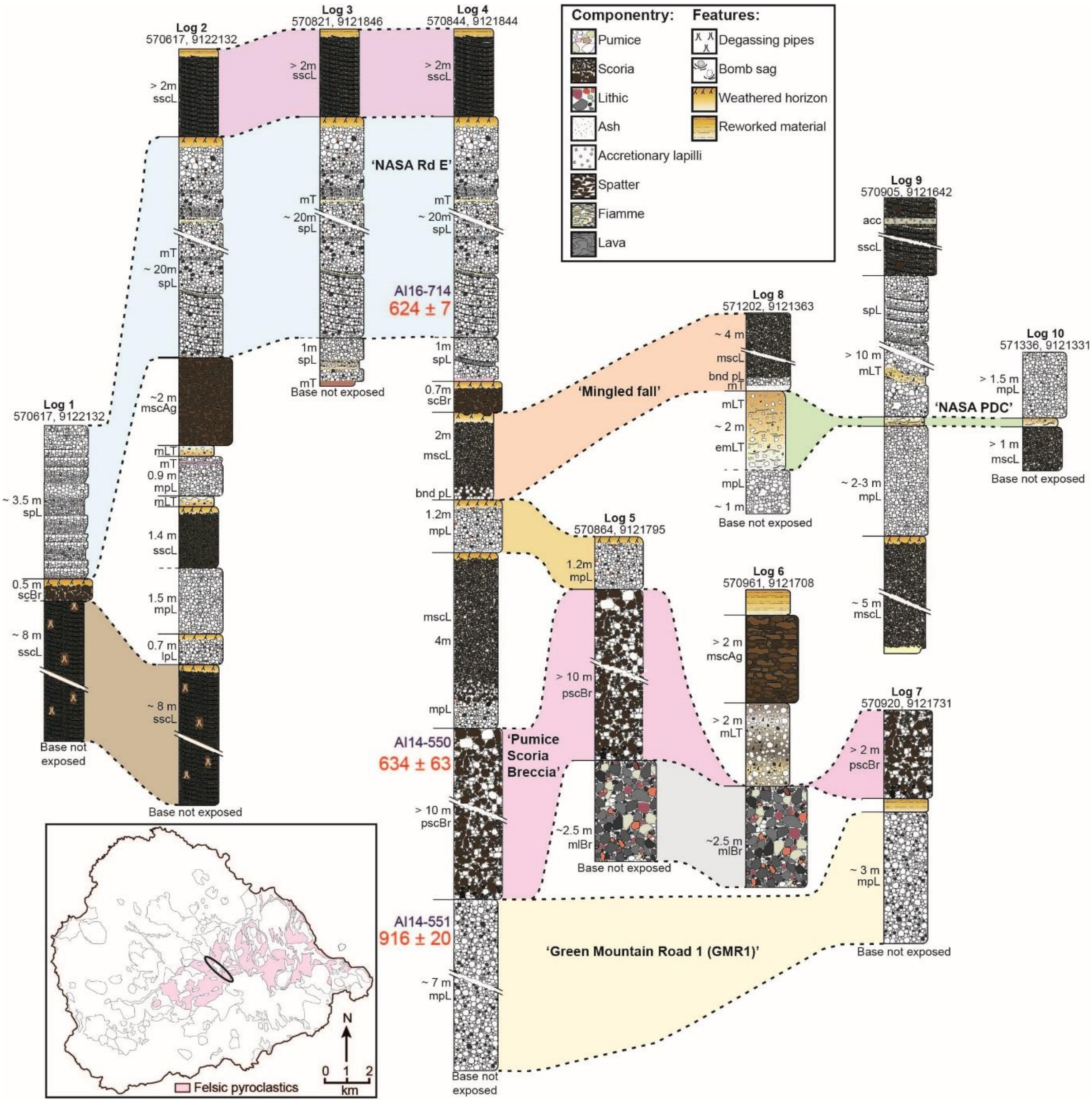

Fig 2: Stratigraphic logs of the pyroclastic products situated on Green Mountain Road. Each unit is labelled with the lithofacies present. Sample numbers are shown for units where XRF and/or $^{40}Ar/^{39}Ar$ data has been collected, and $^{40}Ar/^{39}Ar$ ages (in ka ± 2-sigma analytical uncertainty) are shown.

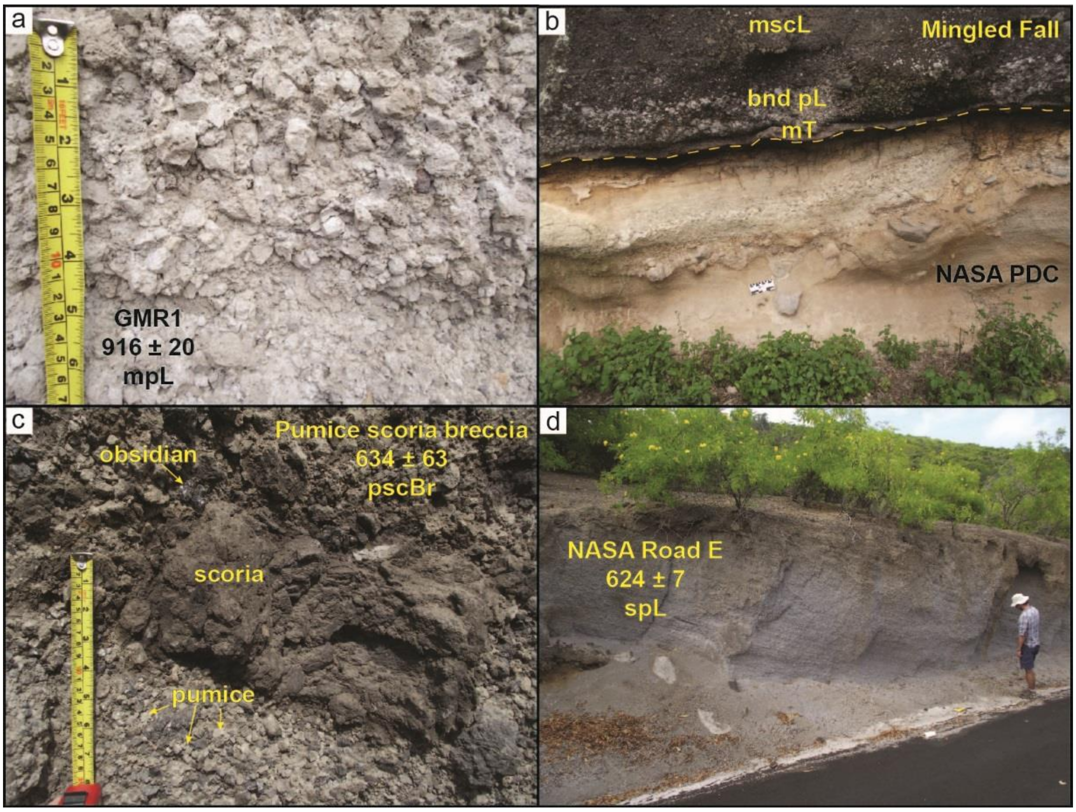

Fig 3: Photographs of Green Mountain Road pyroclastic deposits, showing eruptive units, lithofacies, and $^{40}Ar/^{39}Ar$ ages (in ka ± 2-sigma analytical uncertainty) where relevant: a) GMR1 pumice fall deposit; b) the Mingled Fall unit overlying the NASA PDC deposit on the Residency Track; c) Pumice Scoria Breccia unit, with bombs of scoria, pumice clasts and obsidian clasts; d) part of the NASA Road E unit on Green Mountain Road.

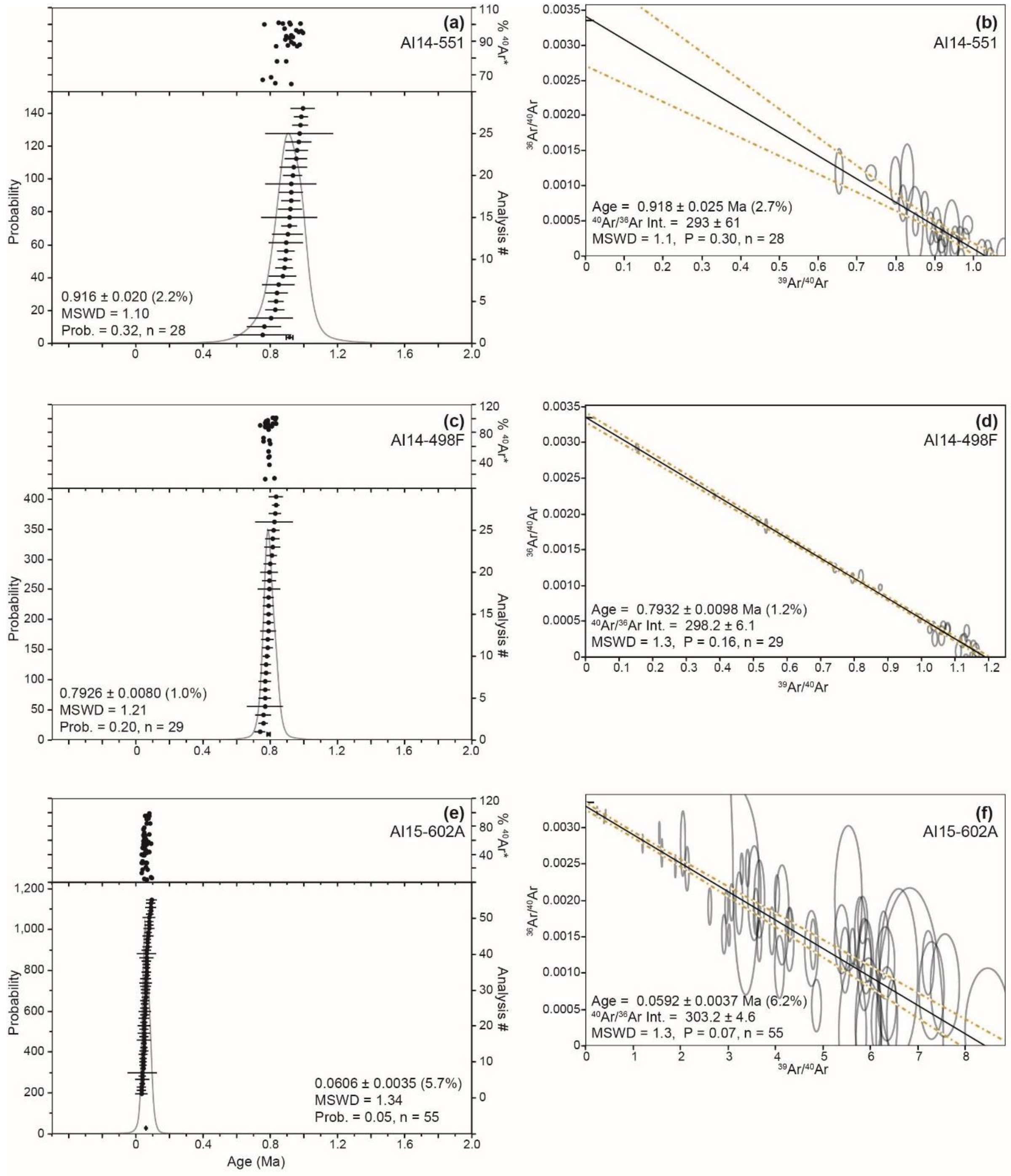

Fig. 4: Example $^{40}Ar/^{39}Ar$ age probability spectra and inverse isochrons. The ages calculated with each method are indistinguishable from each other for all samples: a) age probability spectra for AI14-551 GMR1; b) inverse isochron for AI14-551 GMR1; c) age probability spectra for AI14-498F Upper NASA Road pumice breccia; d) inverse isochron for AI14-498F Upper NASA Road pumice breccia; e,f) age probability spectra and inverse isochron for AI15-602A Echo Canyon eruption. This is an example where the $^{40}Ar/^{36}Ar$ is distinguishable from

atmosphere and therefore the inverse isochron age is more appropriate. See Supplementary Material for all age probability spectra and inverse isochrons and for $^{40}Ar/^{39}Ar$ data.

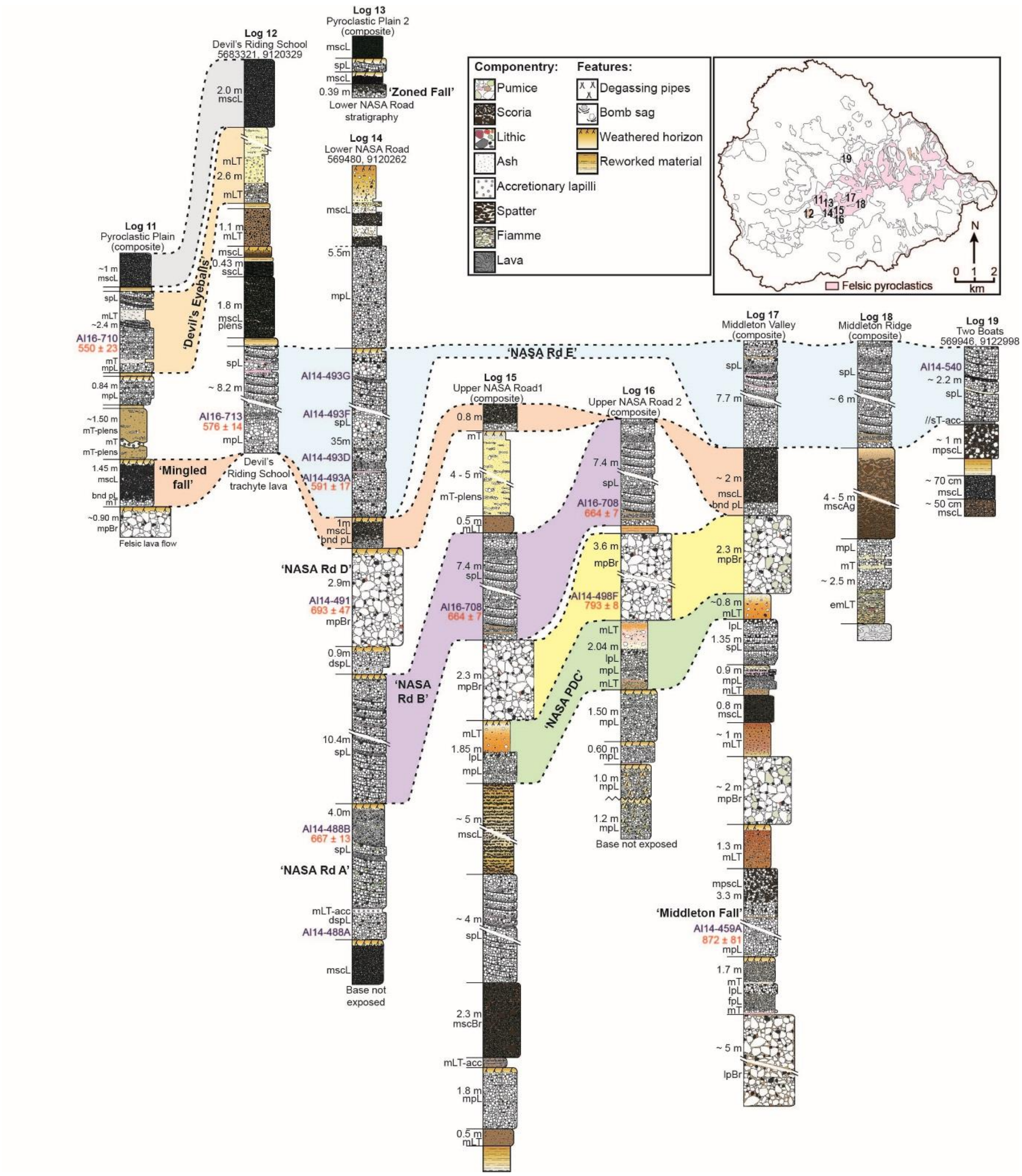

Fig 5: Stratigraphic logs of the pyroclastic products located within the central region of Ascension. Each unit is labelled with the lithofacies present. Sample numbers are shown for

units where XRF and/or $^{40}Ar/^{39}Ar$ data has been collected, and $^{40}Ar/^{39}Ar$ ages (in ka ± 2-sigma analytical uncertainty) are shown.

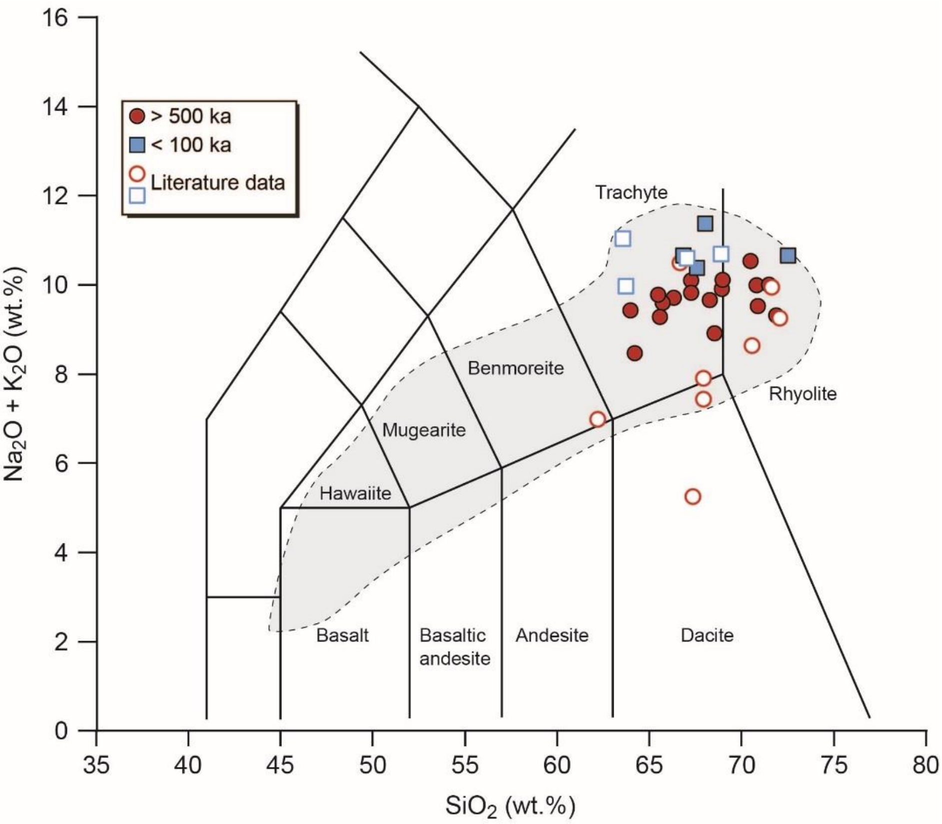

Fig. 6: Total alkali vs. SiO_2 diagram of pumice samples > 500 ka and < 100 ka. Literature pumice XRF data taken from Weaver et al. (1996); Kar et al. (1998); Chamberlain et al. (2016, 2019, 2020). Grey field defines published Ascension XRF data, including lavas and scoria with data from Weaver et al. (1996); Kar et al. (1998); Ammon et al. (2009); Jicha et al. (2013); Chamberlain et al. (2019). All values normalised to 100 wt. % on a volatile-free basis.

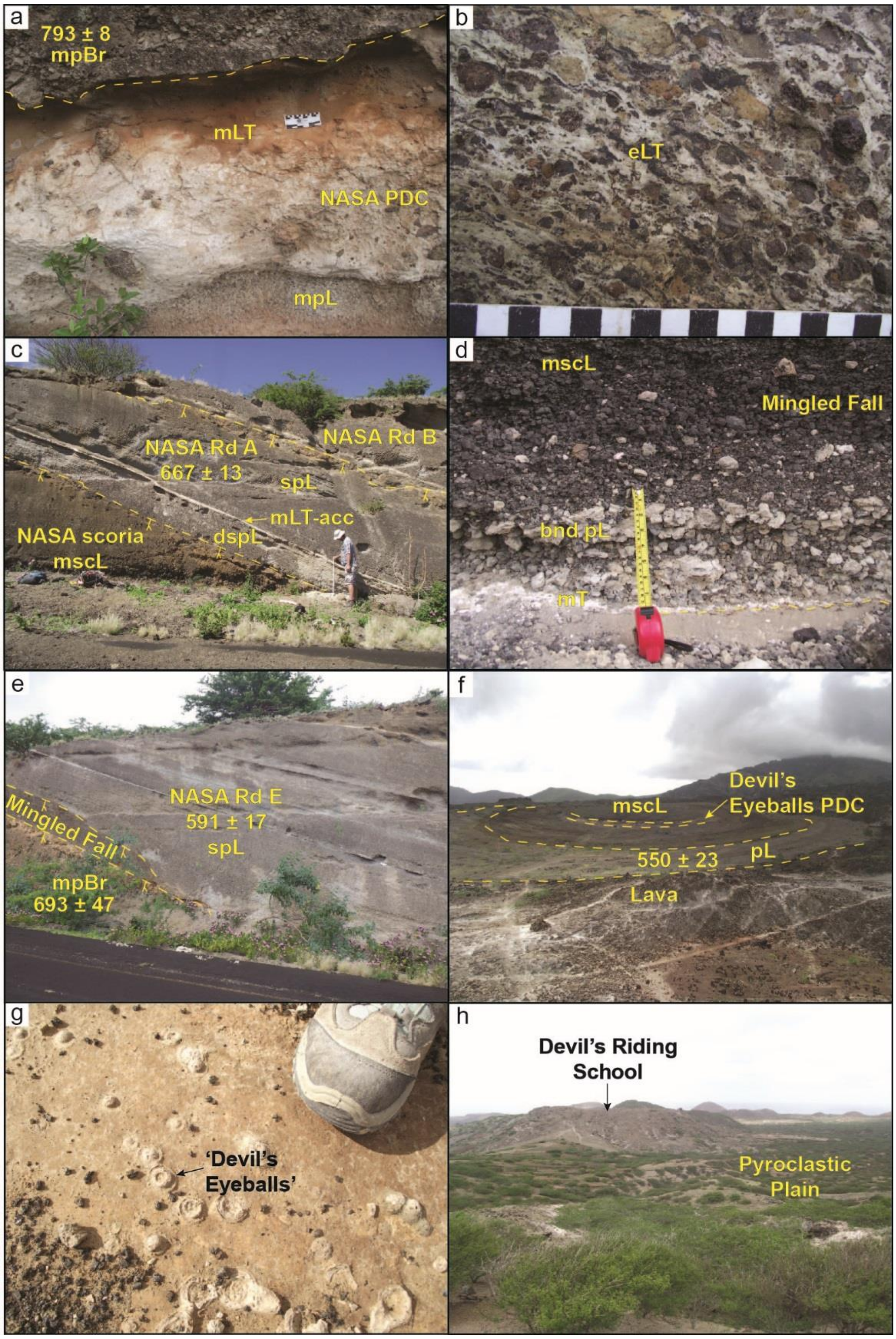

Fig 7: Photographs of pyroclastic deposits located in the centre of Ascension, showing eruptive units, lithofacies, and $^{40}Ar/^{39}Ar$ ages where relevant: a) NASA ignimbrite and overlying pumice breccia situated on Upper NASA Rd; b) eutaxitic, variably welded PDC deposit located near Middleton Ridge; c) Lower NASA Rd sequence – Lower NASA A and B; d) the Mingled

Fall deposit on Pyroclastic Plain; e) Lower NASA Rd sequence – massive pumice breccia, Mingled Fall and NASA Rd E; f) overview of Devil’s Riding School - a crater filled with pyroclastic deposits subsequently eroded to reveal a concentric, inwardly-dipping sequence; g) a view over Pyroclastic Plain and Devil’s Riding School, as seen from Lower NASA Road.

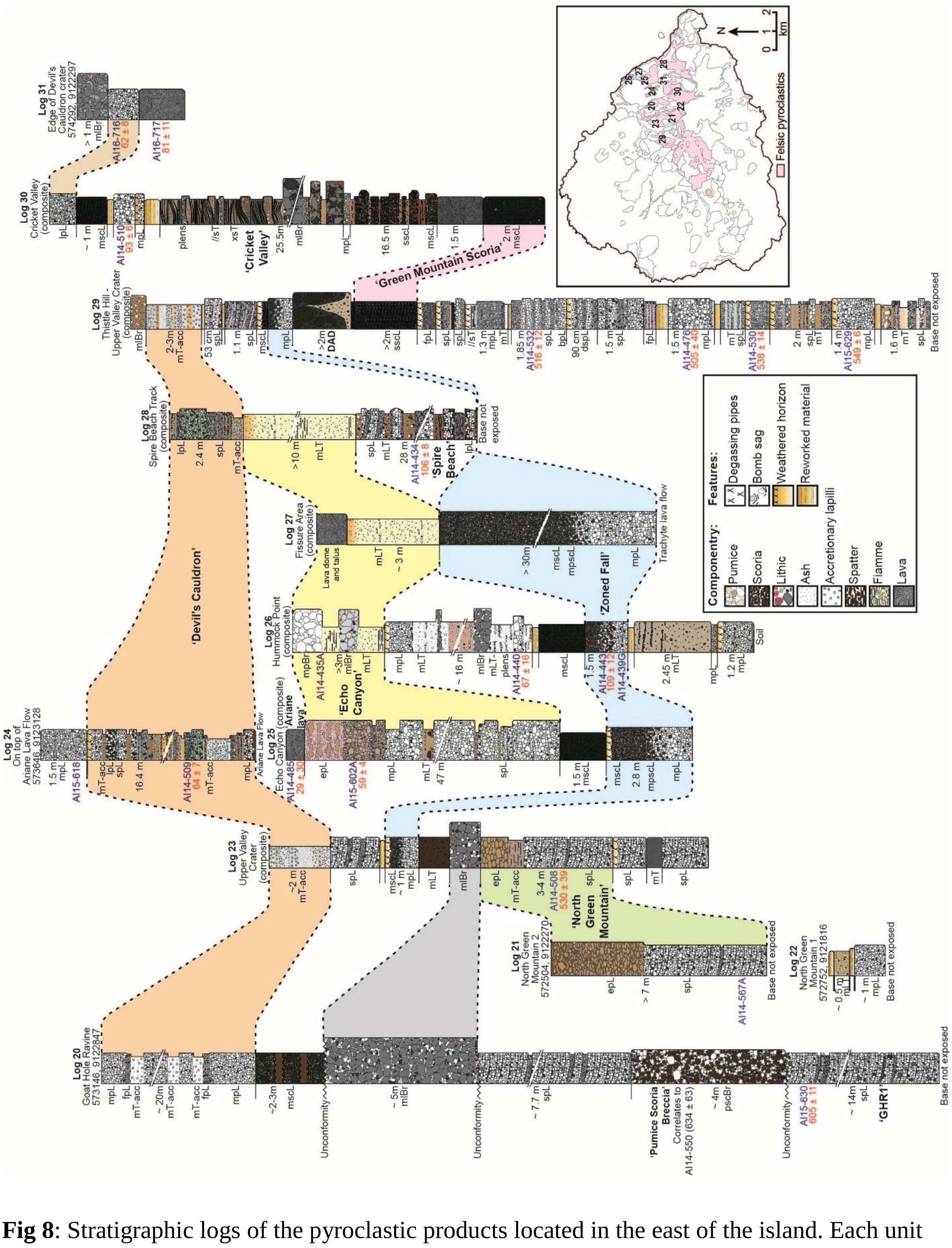

Fig 8: Stratigraphic logs of the pyroclastic products located in the east of the island. Each unit is labelled with the lithofacies present. Sample numbers are shown for units where XRF and/or $^{40}Ar/^{39}Ar$ data has been collected, and $^{40}Ar/^{39}Ar$ ages (in ka ± 2-sigma analytical uncertainty) are shown.

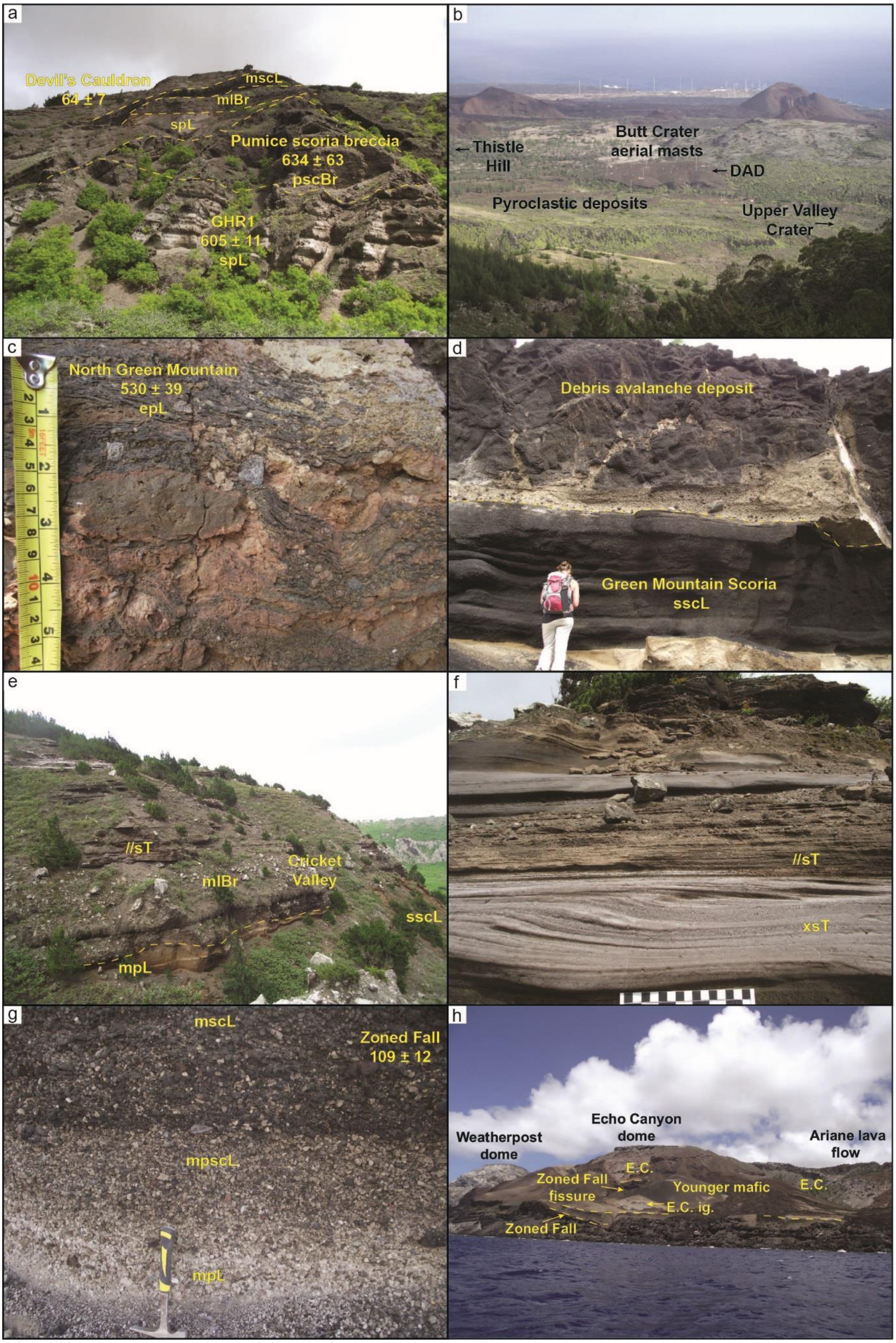
a
Devil's Cauldron
64 ± 7
mscL
mlBr
spL
Pumice scoria breccia
634 ± 63
pscBr
GHR1
605 ± 11
spL
b
Thistle Hill
Butt Crater aerial masts
DAD
Pyroclastic deposits
Upper Valley Crater
c
North Green Mountain
530 ± 39
epL
d
Debris avalanche deposit
Green Mountain Scoria
sscL
e
//sT
mlBr
Cricket Valley
sscL
mpL
f
//sT
xsT
g
mscL
Zoned Fall
109 ± 12
mpscL
mpL
h
Weatherpost dome
Echo Canyon dome
Ariane lava flow
E.C.
Zoned Fall fissure
Younger mafic
E.C. ig.
E.C.
Zoned Fall

992

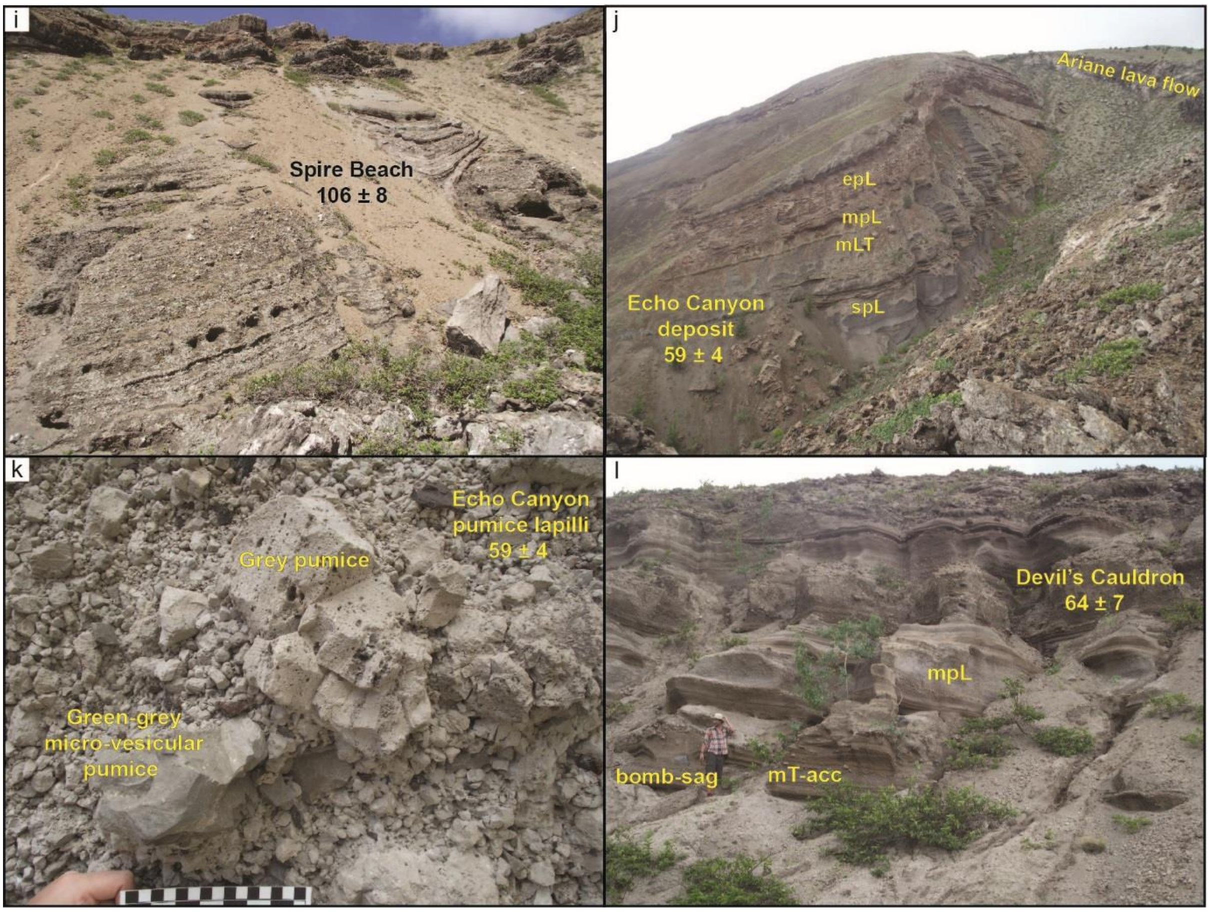

Fig 9: Photographs of pyroclastic deposits situated in the east of Ascension, showing eruptive units, lithofacies, and $^{40}Ar/^{39}Ar$ ages (in ka ± 2-sigma analytical uncertainty) where relevant: a) overview of Goat Hole Ravine section; b) overview of area between Thistle Hill (out of frame) and Upper Valley Crater, viewed from Green Mountain looking towards the northwest. The area is the site of many pyroclastic deposits and the debris avalanche deposit (DAD); c) eutaxitic welded fall forming the top of the North Green Mountain unit exposed in a location on the northern side of Green Mountain; d) Green Mountain Scoria unit and overlying debris avalanche deposit composed of the same scoria; e) Cricket Valley eruption deposit showing massive lithic breccia (mlBr) overlain by stratified (//sT) surge deposits; f) cross- and parallel-stratified tuff (xsT, //sT) deposited by dilute PDCs (surges) during the Cricket Valley eruption; g) the Zoned Fall deposit; h) part of the northeast coast, southeast of Hummock Point, viewed from offshore. The Zoned Fall and its associated fissure region is overlain by the Echo Canyon

(E.C.) eruption deposits (ignimbrite facies and dome), overlain by the Ariane Flow and mafic deposits; i) the Spire Beach tuff cone deposits; j) an overview of Echo Canyon and the Echo Canyon eruption deposits, overlain by the Arine lava flow; k) Echo Canyon pumice fall showing clasts with different vesicularity; l) overview of the Devil's Cauldron unit situated on top of the Ariane lava flow.

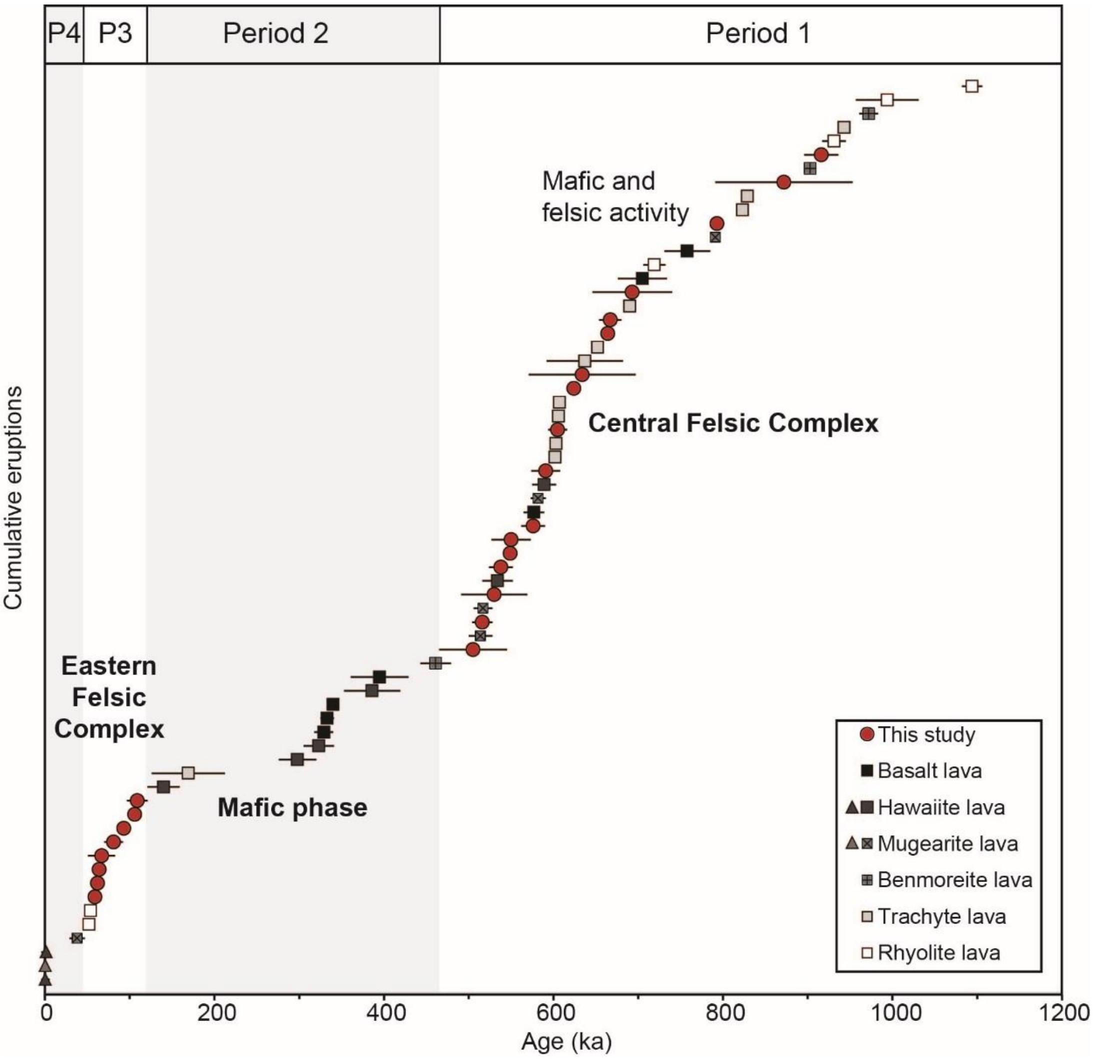

Fig. 10: $^{40}Ar/^{39}Ar$ ages (2σ uncertainty) for all pumice eruptions in this study, with additional lava ages and compositions from Jicha et al., (2013) (squares) and Preece et al. (2018) (triangles). The subaerial eruptive history may be divided into four eruptive periods based on these ages and the stratigraphy. See text for further explanation.